

# Modulation of Type 1 Inositol (1,4,5)-Trisphosphate Receptor Function by Protein Kinase A and Protein Phosphatase 1 $\alpha$

Tie-Shan Tang,\* Huiping Tu,\* Zhengnan Wang, and Ilya Bezprozvanny

Department of Physiology, University of Texas Southwestern Medical Center, Dallas, Texas 75390

Type 1 inositol (1,4,5)-trisphosphate receptors (InsP<sub>3</sub>R1s) play a major role in neuronal calcium (Ca<sup>2+</sup>) signaling. The InsP<sub>3</sub>R1s are phosphorylated by protein kinase A (PKA), but the functional consequences of InsP<sub>3</sub>R1 phosphorylation and the mechanisms that control the phosphorylated state of neuronal InsP<sub>3</sub>R1s are poorly understood. In a yeast two-hybrid screen of rat brain cDNA library with the InsP<sub>3</sub>R1-specific bait, we isolated the protein phosphatase 1 $\alpha$  (PP1 $\alpha$ ). In biochemical experiments, we confirmed the specificity of the InsP<sub>3</sub>R1–PP1 $\alpha$  association and immunoprecipitated the InsP<sub>3</sub>R1–PP1 complex from rat brain synaptosomes and from the neostriatal lysate. We also established that the association with PP1 facilitates dephosphorylation of PKA-phosphorylated InsP<sub>3</sub>R1 by the endogenous neostriatal PP1 and by the recombinant PP1 $\alpha$ . We demonstrated that exposure of neostriatal slices to 8-bromo-cAMP, dopamine, calyculin A, or cyclosporine A, but not to 10 nM okadaic acid, promotes the phosphorylation of neostriatal InsP<sub>3</sub>R1 by PKA *in vivo*. We discovered that PKA activates and PP1 $\alpha$  inhibits the activity of recombinant InsP<sub>3</sub>R1 reconstituted into planar lipid bilayers. We found that phosphorylation of InsP<sub>3</sub>R1 by PKA induces at least a fourfold increase in the sensitivity of InsP<sub>3</sub>R1 to activation by InsP<sub>3</sub> without shifting the peak of InsP<sub>3</sub>R1 bell-shaped Ca<sup>2+</sup> dependence. Based on these data, we suggest that InsP<sub>3</sub>R1 may participate in cross talk between cAMP and Ca<sup>2+</sup> signaling in the neostriatum and possibly in other regions of the brain.

**Key words:** inositol trisphosphate receptor; calcium signaling; dopamine; protein phosphorylation; yeast two-hybrid; planar lipid bilayers

## Introduction

Calcium ions (Ca<sup>2+</sup>) are universal second messengers. Changes in cytosolic Ca<sup>2+</sup> concentration influence most fundamental cellular processes in neuronal and non-neuronal cells (Berridge, 1993, 1998). Inositol 1,4,5-trisphosphate (InsP<sub>3</sub>), a soluble compound generated by enzymatic cleavage of the lipid phosphatidylinositol 4,5-bisphosphate after activation of phospholipase C (PLC), is a second messenger used by many cell types to stimulate Ca<sup>2+</sup> release from intracellular Ca<sup>2+</sup> stores. InsP<sub>3</sub>-induced Ca<sup>2+</sup> release in these cells is supported by a highly specialized Ca<sup>2+</sup> channel, the inositol (1,4,5)-trisphosphate receptor (InsP<sub>3</sub>R). Three mammalian isoforms of InsP<sub>3</sub>R have been identified, each with the unique expression pattern (for review, see Furuichi et al., 1994; Taylor et al., 1999). The three mammalian InsP<sub>3</sub>R isoforms share 60–70% amino acid homology, but the differences in their functional properties are poorly understood (for review, see Thrower et al., 2001). The type 1 InsP<sub>3</sub>R (InsP<sub>3</sub>R1) is a predominant isoform in the CNS. Targeted deletion of *InsP<sub>3</sub>R1* gene in

mouse induces ataxia and epileptic seizures, followed by a premature death (Matsumoto et al., 1996), highlighting the importance of InsP<sub>3</sub>R1 for brain function.

InsP<sub>3</sub>R1s are subjected to multiple levels of regulation in cells (Bezprozvanny and Ehrlich, 1995). Binding of InsP<sub>3</sub> triggers the InsP<sub>3</sub>R1 channel opening. The activity of InsP<sub>3</sub>R1 is under feedback control by cytosolic Ca<sup>2+</sup>; at low Ca<sup>2+</sup> concentrations, Ca<sup>2+</sup> acts as a coactivator of the InsP<sub>3</sub>R1, and at high Ca<sup>2+</sup> concentrations, the InsP<sub>3</sub>R1 is inhibited by Ca<sup>2+</sup> (Iino, 1990; Bezprozvanny et al., 1991; Finch et al., 1991; Kaznatcheyeva et al., 1998). The activity of InsP<sub>3</sub>R1 is allosterically potentiated by ATP (Ferris et al., 1990; Iino, 1991; Bezprozvanny and Ehrlich, 1993). The InsP<sub>3</sub>R1 is also one of the major substrates of protein kinase A (PKA) phosphorylation in the brain (Walaas et al., 1986; Supattapone et al., 1988; Maeda et al., 1990; Danoff et al., 1991; Ferris et al., 1991a; Haug et al., 1999; Pieper et al., 2001). PKA can phosphorylate InsP<sub>3</sub>R1 at two sites, S1589 and S1755 (Danoff et al., 1991; Ferris et al., 1991a; Haug et al., 1999; Pieper et al., 2001). Both sites are located in the coupling domain of the InsP<sub>3</sub>R1 (Furuichi et al., 1994), and PKA phosphorylation is likely to affect InsP<sub>3</sub>R1 function. However, functional consequences of neuronal InsP<sub>3</sub>R1 phosphorylation by PKA remain controversial. An activation (Volpe and Alderson-Lang, 1990; Nakade et al., 1994; Wojcikiewicz and Luo, 1998) or an inhibition (Supattapone et al., 1988; Cameron et al., 1995) of InsP<sub>3</sub>R1 by PKA was observed using Ca<sup>2+</sup> flux measurements.

What are the mechanisms that control phosphorylation of InsP<sub>3</sub>R1 by PKA in the brain? What are the functional consequences of InsP<sub>3</sub>R1 phosphorylation by PKA? Is modulation of

Received June 3, 2002; revised Oct. 29, 2002; accepted Oct. 30, 2002.

This work was supported by the Welch Foundation and National Institutes of Health Grant R01 NS38082 (I.B.). The initial yeast two-hybrid screen was performed by Dale Elmer and Anton Maximov. We are grateful to them for their effort. We are thankful to Thomas C. Südhof, Anton Maximov, and Elena Nosyreva for many helpful discussions and valuable experimental advice and to Phyllis Foley for expert administrative assistance. We thank Thomas C. Südhof for the rat InsP<sub>3</sub>R1 clone and the rat brain cDNA library, Gregory Mignery for the rat InsP<sub>3</sub>R2 clone, Graeme Bell for the rat InsP<sub>3</sub>R3 clone, and Jan Parys for the cyt13b2 antibody.

\*T.-S.T. and H.T. contributed equally to this work.

Correspondence should be addressed to Dr. Ilya Bezprozvanny, Department of Physiology, K4.112, University of Texas Southwestern Medical Center, 5323 Harry Hines Boulevard, Dallas, TX 75390-9040. E-mail: Ilya.Bezprozvanny@UTSouthwestern.edu.

Copyright © 2003 Society for Neuroscience 0270-6474/03/230403-13\$15.00/0

neuronal InsP<sub>3</sub>R1 function by PKA physiologically relevant? Here we address some of these questions. In a yeast two-hybrid screen of rat brain cDNA library with the InsP<sub>3</sub>R1-specific bait, we isolated a cDNA of protein phosphatase 1 $\alpha$  (PP1 $\alpha$ ). In a series of biochemical and electrophysiological *in vitro* experiments, we analyzed the importance of InsP<sub>3</sub>R1–PP1 $\alpha$  association for control of InsP<sub>3</sub>R1 phosphorylation by PKA and modulation of InsP<sub>3</sub>R1 activity. In addition, we characterized the phosphorylation of InsP<sub>3</sub>R1 by PKA during neostriatal dopaminergic signaling *in vivo*. Our results suggest that InsP<sub>3</sub>R1 may play a role in the cross talk between cAMP and Ca<sup>2+</sup> signaling pathways in the neostriatum (Greengard et al., 1999) and possibly in other regions of the brain.

## Materials and Methods

**Yeast two-hybrid methods.** The C-terminal regions of rat InsP<sub>3</sub>R1 (Mignery et al., 1990) (amino acids Q2714–A2749), rat InsP<sub>3</sub>R2 (Sudhof et al., 1991) (amino acids Q2666–H2701), and rat InsP<sub>3</sub>R3 (Blondel et al., 1993) (amino acids Q2641–R2670) were amplified by PCR and cloned into pLexN vector to yield IC1, IC2, and IC3 baits. Mutant and truncated versions of IC1 bait were generated by PCR and verified by sequencing. The yeast two-hybrid screen of rat brain cDNA library in pVp16-3 vector ( $3 \times 10^5$  independent clones; gift from Dr T. Südhof, University of Texas Southwestern Medical Center, Howard Hughes Medical Institute, Dallas, TX) with IC1 bait was performed according to published procedures (Hata et al., 1996). Coding sequences of mouse PP1 $\beta$  and human PP1 $\gamma$  were amplified by PCR from expressed sequence tags (ESTs) (GenBank accession numbers BF179322 and BG389563) and subcloned into pVp16-3 prey vector. The liquid yeast two-hybrid assays were performed as described previously (Maximov et al., 1999).

**In vitro binding assay.** RIGLLGHPPHMNVNPPQQA (RIGL-V1, 2731–2749 of rat InsP<sub>3</sub>R1), RLGFLGSNTPHENHHMPPH (RLGF-V2, 2683–2701 of rat InsP<sub>3</sub>R2), and RLGFDVQNCMSR (RLGF-V3, 2658–2670 of rat InsP<sub>3</sub>R3) peptides were synthesized and coupled to *N*-hydroxysuccinimide (NHS)-activated Sepharose according to the manufacturer's (Amersham Biosciences, Uppsala, Sweden) instructions. The rat PP1 $\alpha$  was cloned into hemagglutinin (HA)-pCMV5 vector (Maximov et al., 1999), expressed in COS7 cells by DEAE–dextran transient transfection, and solubilized in the extraction buffer A [1% 3-[(3-cholamidopropyl)dimethylammonio]-1-propanesulfonate (CHAPS), 137 mM NaCl, 2.7 mM KCl, 4.3 mM Na<sub>2</sub>HPO<sub>4</sub>, 1.4 mM KH<sub>2</sub>PO<sub>4</sub>, 5 mM EDTA, 5 mM EGTA, and protease inhibitors]. The HA–PP1 $\alpha$ -containing extract was clarified by 20 min of centrifugation (100,000  $\times$  g in TL-100) and incubated with RIGL-V1, RLGF-V2, and RLGF-V3 Sepharose beads for 16 hr at 4°C. Beads were washed with 40 bead volumes of the extraction buffer A, and attached proteins were sequentially eluted with 1 bead volume of 1 M NaCl and then 1 bead volume of 1% SDS. Samples were resolved by SDS-PAGE and analyzed by immunoblotting with anti-HA antibodies.

**Immunoprecipitations.** The RT1 baculovirus encoding the SI(–)/SII(+) splice variant of rat InsP<sub>3</sub>R1 (Mignery et al., 1990) has been described previously (Tu et al., 2002). The RT1 $\Delta$ C baculovirus encoding rat InsP<sub>3</sub>R1 truncated at position G2736 was generated using the Bac-to-Bac system (Invitrogen, San Diego, CA) as described previously (Tu et al., 2002). High Five (Invitrogen) or Sf9 (American Type Culture Collection, Manassas, VA) insect cells were infected with high titer ( $>10^8$  colony-forming units/ml) stocks of RT1 and RT1 $\Delta$ C baculoviruses as described previously (Tu et al., 2002). At 48 hr after infection, the insect cells were solubilized in the extraction buffer A. Rat PP1 $\alpha$ , mouse PP1 $\beta$ , and human PP1 $\gamma$  were amplified by PCR from ESTs, cloned into HA–pCMV vector (Maximov et al., 1999), expressed in COS7 cells by DEAE–dextran transient transfection, and solubilized in the extraction buffer A. Extracts from Sf9 cells and COS7 cells were clarified by centrifugation (100,000  $\times$  g in TL-100), mixed together, and immunoprecipitated for 2 hr at 4°C with anti-HA monoclonal antibodies (mAbs) attached to protein G-agarose beads. mAb against InsP<sub>3</sub>R1 was used as a positive control. The amount of precipitated InsP<sub>3</sub>R1 was quantified by [<sup>3</sup>H]InsP<sub>3</sub> bind-

ing as described previously (Kaznatcheyeva et al., 1998). Glutathione S-transferase (GST), GST–IC1, GST–IC2, and GST–IC3 fusion proteins (in pGEX-KG; Amersham Biosciences) were expressed in BL21 cells, purified on glutathione beads as described previously (Maximov et al., 1999), and added to immunoprecipitation reactions at a concentration of 200  $\mu$ g/ml. Cortex rat brain synaptosomes and rat neostriatum homogenates were prepared according to published procedures (Jones and Matus, 1974; Nishi et al., 1997; Maximov et al., 1999) and verified by Western blotting with anti-postsynaptic density 95 (PSD95) and anti-dopamine and cAMP-regulated phosphoprotein (DARPP)-32 polyclonal antibodies, respectively. The synaptosomes and neostriatum homogenates were solubilized in extraction buffer A, clarified by centrifugation (100,000  $\times$  g in TL-100), and immunoprecipitated with anti-InsP<sub>3</sub>R1 T443 polyclonal antibodies attached to protein A-Sepharose beads. The precipitate was analyzed by Western blotting with mAbs against PP1.

**In vitro dephosphorylation assay.** Recombinant RT1 and RT1 $\Delta$ C were precipitated from insect cell extracts with the anti-InsP<sub>3</sub>R1 polyclonal antibodies (T443 or cytl3b2, respectively) attached to protein A-Sepharose beads and phosphorylated as described previously (Wojcikiewicz and Luo, 1998). Briefly, precipitated RT1 or RT1 $\Delta$ C was washed three times with the ice-cold phosphorylation buffer (120 mM KCl, 50 mM Tris, pH 7.2, 0.3 mM MgCl<sub>2</sub>, 0.1% Triton X-100) and resuspended in the phosphorylation buffer. The phosphorylation reaction was initiated by addition of 5  $\mu$ Ci [ $\gamma$ -<sup>32</sup>P]ATP, 5  $\mu$ M ATP, and 10 U of PKA bovine heart catalytic subunit in 200  $\mu$ l volume; continued for 1 hr at 30°C; and stopped by addition of 1.3 ml of ice-cold phosphorylation buffer containing 2 mM ATP. The beads were pelleted, washed two times with the dephosphorylation buffer I (50 mM NaCl, 50 mM Tris, pH 7.2, 0.7 mg/ml BSA, 3.3 mM caffeine, 0.15 mM MnCl<sub>2</sub>, 1.0 mM DTT), and resuspended in 100  $\mu$ l of the dephosphorylation buffer I. The dephosphorylation reactions were initiated by addition of 0.1 U of rabbit recombinant PP1 $\alpha$  or  $2 \times 10^{-4}$  U of human recombinant PP1 $\gamma$  (both from Calbiochem, La Jolla, CA), incubated at 30°C for 0–40 min, and stopped by addition of 5 mM EDTA.

The rat neostriatum homogenate prepared as described previously (Nishi et al., 1999) was used as a source of endogenous PP1 activity (nsPP1). The dephosphorylation reactions with nsPP1 were performed in dephosphorylation buffer II (50 mM Tris–Cl, 50 mM NaCl, pH 7.2, 0.1 mM EGTA, 1 mM okadaic acid, 1 mM DTT, 0.7 mg/ml BSA, 3.3 mM caffeine). The nsPP1 dephosphorylation reactions were initiated by addition of 4  $\mu$ g of striatal homogenate and stopped by addition of 1.4 ml of ice-cold dephosphorylation buffer II, brief centrifugation, and rapid (within 3 min) addition of equal volume of 2 $\times$  SDS-gel loading buffer. Resulting samples were boiled for 5 min, separated by SDS-electrophoresis on 8% polyacrylamide gel, and analyzed by phosphorimaging (Bio-Rad, Richmond, CA). GST/GST–IC1 (200  $\mu$ g/ml), DARPP-32/pDARPP-32 (0.2  $\mu$ M), or PP1 inhibitor-2 (Inh2) (0.2  $\mu$ M) were added to dephosphorylation reactions as indicated in Results.

**Neostriatal InsP<sub>3</sub>R1 back-phosphorylation.** The neostriatum of adult rats was dissected (Nishi et al., 1997), chopped into small slices ( $\sim 1$ – $2 \times 1$ – $2$  mm) in ice-cold, oxygenated (95%O<sub>2</sub>–5% CO<sub>2</sub>) Krebs–HCO<sub>3</sub><sup>–</sup> buffer, aliquoted, washed, and preincubated in 5 ml of fresh Krebs–HCO<sub>3</sub><sup>–</sup> buffer at 30°C under constant oxygenation for 60 min, with a single change of medium. The neostriatum slices were then placed into fresh Krebs–HCO<sub>3</sub><sup>–</sup> buffer containing 20  $\mu$ M IBMX and treated with 8-bromo-cAMP (8-Br-cAMP), dopamine, cyclosporine A, calyculin A, or okadaic acid as indicated in Results. After the drug treatment, the pieces were collected, homogenized, and solubilized in the extraction buffer A containing 0.5 mM Na<sub>3</sub>VO<sub>4</sub>. The extracts were clarified by centrifugation (100,000  $\times$  g in TL-100), and protein concentration in lysates was determined by Bio-Rad assay. The equal amounts of protein from each lysate were used for immunoprecipitation with anti-InsP<sub>3</sub>R1 T443 polyclonal antibodies attached to protein A-Sepharose beads. The precipitated InsP<sub>3</sub>R1s were phosphorylated *in vitro* by the catalytic subunit of PKA in the presence of [ $\gamma$ -<sup>32</sup>P]ATP and analyzed by phosphorimaging as described above. When the neostriatal lysate was dephosphorylated by PP1 $\alpha$  before *in vitro* phosphorylation by PKA, the measured content of the <sup>32</sup>P-InsP<sub>3</sub>R1 band (<sup>32</sup>P<sub>PP1 $\alpha$</sub> ) was interpreted as total InsP<sub>3</sub>R1 in the

neostriatal sample. To calculate the fraction of InsP<sub>3</sub>R1 in the PKA-phosphorylated state, the <sup>32</sup>P content of the InsP<sub>3</sub>R1 band at each data point (<sup>32</sup>P-InsP<sub>3</sub>R1) was normalized to the total InsP<sub>3</sub>R1 content, as follows: pInsP<sub>3</sub>R1 = (<sup>32</sup>P<sub>PP1 $\alpha$</sub>  - <sup>32</sup>P-InsP<sub>3</sub>R1) / <sup>32</sup>P<sub>PP1 $\alpha$</sub> .

**Planar lipid bilayer experiments.** Single-channel recordings of recombinant RT1 or RT1 $\Delta$ C activity were performed as described previously (Tu et al., 2002) at 0 mV transmembrane potential using 50 mM Ba<sup>2+</sup> dissolved in HEPES, pH 7.35, in the *trans* (intraluminal) side as a charge carrier. The *cis* (cytosolic) chamber contained 110 mM Tris dissolved in HEPES, pH 7.35, -log ([Ca<sup>2+</sup>]) (pCa) 6.7 (0.2 mM EGTA plus 0.14 mM CaCl<sub>2</sub>) (Bezprozvanny et al., 1991), and 3% sucrose. InsP<sub>3</sub>R1s were activated by addition of 2  $\mu$ M InsP<sub>3</sub> (Alexis) to the *cis* chamber. The *cis* chamber contained 0.5 mM MgATP or 0.3 mM MgCl<sub>2</sub> plus 0.1 mM Li<sub>4</sub>ATP $\gamma$ S as indicated in Results. PKA bovine heart catalytic subunit was diluted in 110 mM Tris/HEPES, pH 7.35, containing 0.2 mM ruthenium red to 2 U/ $\mu$ l. Rabbit recombinant PP1 $\alpha$  was diluted in 110 mM Tris/HEPES, pH 7.35, containing 0.2 mM ruthenium red and 0.2 mM MnCl<sub>2</sub> to 1 U/ $\mu$ l. One microliter of PKA or PP1 $\alpha$  stocks was added directly to the bilayer without stirring. The phosphorylation/dephosphorylation reactions were stopped 1 min after PKA/PP1 $\alpha$  addition by stirring the solution in the *cis* chamber for 30 sec. Stirring resulted in a 3000-fold reduction of PKA/PP1 $\alpha$  concentration (1  $\mu$ l in 3 ml dilution), greatly reducing the rate of InsP<sub>3</sub>R1 phosphorylation/dephosphorylation in the bilayer. In Ca<sup>2+</sup>-dependence experiments, the free Ca<sup>2+</sup> concentration in the *cis*-chamber was controlled in the range of 10 nM (pCa 8) to 10  $\mu$ M (pCa 5) by a mixture of 1 mM EGTA, 1 mM HEDTA, and variable concentrations of CaCl<sub>2</sub>. The resulting free Ca<sup>2+</sup> concentration was calculated by using a program described by Fabiato (1988). InsP<sub>3</sub> dependence was measured by consecutive addition of InsP<sub>3</sub> to the *cis* chamber from 1 mM stock. All additions (InsP<sub>3</sub>, ATP, CaCl<sub>2</sub>) were to the *cis* chamber from the concentrated stocks, with at least 30 sec of stirring of solutions in both chambers. The InsP<sub>3</sub>R1 single-channel currents were amplified (OC-725; Warner Instruments, Hamden, CT), filtered at 1 kHz with a low-pass eight pole Bessel filter, digitized at 5 kHz (Digidata 1200; Axon Instruments, Foster City, CA), and stored on computer hard drive and recordable optical disks.

For off-line computer analysis (pClamp 6; Axon Instruments) single-channel data were filtered digitally at 500 Hz; for presentation of the current traces, data were filtered at 200 Hz. Evidence for the presence of two to three functional channels in the bilayer was obtained in the majority of experiments. The number of active channels in the bilayer was estimated as a maximal number of simultaneously open channels during the course of an experiment (Horn, 1991). The open probability of closed level and first and second open levels was determined by using half-threshold crossing criteria ( $t \geq 2$  msec) from the records lasting at least 2.5 min. The single-channel open probability ( $P_o$ ) for one channel was calculated using the binomial distribution for the levels 0, 1, and 2, assuming that the channels were identical and independent (Colquhoun and Hawkes, 1983). To construct InsP<sub>3</sub> and Ca<sup>2+</sup> dependence curves for the InsP<sub>3</sub>R1 in control and PKA-phosphorylated states, the determined values of  $P_o$  were averaged across several independent experiments at each InsP<sub>3</sub> or Ca<sup>2+</sup> concentration. For InsP<sub>3</sub>-dependence experiments, the averaged values of  $P_o$  are presented as mean  $\pm$  SE ( $n$  = number of independent experiments) and fit by the following equation:  $P_o$  (InsP<sub>3</sub>) =  $P_{max}$  (InsP<sub>3</sub>) <sup>$n$</sup>  / [(InsP<sub>3</sub>) <sup>$n$</sup>  +  $k_{InsP_3}$  <sup>$n$</sup> ], modified from Lupu et al. (1998), where  $P_{max}$  is a maximal  $P_o$  value,  $n$  is a Hill coefficient, and  $k_{InsP_3}$  is the apparent affinity of InsP<sub>3</sub>R1 for InsP<sub>3</sub>. For Ca<sup>2+</sup>-dependence experiments, the averaged values of  $P_o$  are presented as mean  $\pm$  SE ( $n$  = number of independent experiments) and fit by the following bell-shaped equation:  $P_o$  (Ca<sup>2+</sup>) =  $4P_m k^n$  (Ca<sup>2+</sup>) <sup>$n$</sup>  / [( $k^n$  + [Ca<sup>2+</sup>] <sup>$n$</sup> ) (K <sup>$n$</sup>  + [Ca<sup>2+</sup>] <sup>$n$</sup> )], modified from Bezprozvanny et al. (1991), where  $P_m$  is a parameter proportional to the maximal  $P_o$  value,  $n$  is a Hill coefficient,  $k$  is the apparent affinity of the Ca<sup>2+</sup> activating site, and  $K$  is the apparent affinity of the Ca<sup>2+</sup> inhibitory site. The fitting procedure used in this study differs from the procedure used in our previous studies (Bezprozvanny et al., 1991; Kaznacheyeva et al., 1998; Lupu et al., 1998; Nosyreva et al., 2002; Tu et al., 2002) in that  $P_o$  values in the present study were not normalized to the maximal  $P_o$  before averaging and fitting. Because  $P_o$

values were not normalized,  $P_m$  is equal to maximal  $P_o$  when  $k = K$ . If  $k \neq K$ ,  $P_m$  is proportional (and higher) than maximal  $P_o$ .

**Materials.** The following mAbs were used: anti-HA for HA.11 (Covance), anti-InsP<sub>3</sub>R1 (Calbiochem), and anti-PP1 mAb (Transduction Laboratories, Lexington, KY). The following polyclonal antibodies were used: C-terminal anti-InsP<sub>3</sub>R1 T443 (Kaznacheyeva et al., 1998), N-terminal anti-InsP<sub>3</sub>R1 cytl3b2 (gift from J. Parys, Ku Leuven, Belgium) (Sipma et al., 1999), anti-PSD95 (gift from T. Südhof), and anti-DARPP-32 (Cell Signaling Technologies). Protein G-agarose beads were supplied by Santa Cruz Biotechnology (Santa Cruz, CA); protein A-Sepharose beads and [ $\gamma$ -<sup>32</sup>P]ATP were obtained from Amersham Biosciences; rabbit recombinant PP1 $\alpha$ , human recombinant PP1 $\gamma$ , DARPP-32, pDARPP-32, PP1 inhibitor-2, calyculin A, and okadaic acid were obtained from Calbiochem, and InsP<sub>3</sub> was supplied by Alexis. PKA bovine heart catalytic subunit, Li<sub>4</sub>ATP $\gamma$ S, and all other reagents are from Sigma (St. Louis, MO).

## Results

### InsP<sub>3</sub>R1 specifically binds PP1 $\alpha$

Each of three mammalian InsP<sub>3</sub>R isoforms contains a unique cytosolic C-terminal tail preceded by a highly conserved region (Fig. 1*a*). To search for the InsP<sub>3</sub>R1-specific neuronal binding partners, we performed a yeast two-hybrid screen of rat brain cDNA library with the IC1 bait (amino acids Q2714-A2749 of rat InsP<sub>3</sub>R1) (Fig. 1*a*) and isolated the full-length clone of PP1 $\alpha$ . When the corresponding regions of InsP<sub>3</sub>R2 (IC2) and InsP<sub>3</sub>R3 (IC3) (Fig. 1*a*) were tested in a liquid yeast two-hybrid assay, we found that PP1 $\alpha$  did not bind IC2 and only weakly associated with IC3 (Fig. 1*b*). Three isoforms of PP1 are expressed in mammalian brain, each with a unique expression pattern (da Cruz e Silva et al., 1995). In a yeast two-hybrid assay, IC1 associated with PP1 $\alpha$  but not with PP1 $\beta$  or PP1 $\gamma$  (Fig. 1*b*). No interaction of IC2 or IC3 baits with PP1 $\beta$  or PP1 $\gamma$  was detected in our yeast two-hybrid experiments (Fig. 1*b*). Thus, the association appears to be specific for the InsP<sub>3</sub>R1-PP1 $\alpha$  pair.

The PP1-targeting proteins share the R/K-V/I-X-F docking motif (Greengard et al., 1999). A similar RIGL motif is present within IC1 sequence (Fig. 1*a*, indicated by a *bar*). However, a similar RLGF motif is also present in IC2 and IC3 sequences (Fig. 1*a*), which are not strong PP1 $\alpha$ -binding partners (Fig. 1*b*). Where is a specific PP1 $\alpha$ -binding site in the IC1 sequence? To address this question, we performed a systematic analysis of PP1 $\alpha$  binding specificity by liquid yeast two-hybrid assay. From sequence alignment of InsP<sub>3</sub>R isoforms, we reasoned that the InsP<sub>3</sub>R C-terminal sequence could be divided into a conserved (C) domain, RXGX motif, and variable (V) regions (Fig. 1*a*). A deletion of conserved domain had no effect on IC1 association with PP1 $\alpha$  (Fig. 2*a*), indicating that the RIGL motif and V1 variable domain (RIGL-V1) is sufficient for association with PP1 $\alpha$ . In contrast, the corresponding regions of IC2 and IC3 baits (RLGF-V2 and RLGF-V3) did not bind PP1 $\alpha$  (Fig. 2*a*), confirming a specificity of the interaction. To determine a role for the RIGL motif in specific association with PP1 $\alpha$ , we generated a series of IC1 bait point mutants and tested them in a yeast two-hybrid assay with PP1 $\alpha$  prey. We found that in the context of the IC1 bait, mutations of RIGL motif to RIGA or RAGL had no apparent effect on the strength of interactions with PP1 $\alpha$  (Fig. 2*a*, *bold* indicates mutated residues). In fact, mutations of the RIGL motif to the RLGF motif present in IC2 and IC3 baits or to the RIGF motif corresponding to the "canonical" PP1 docking motif (Greengard et al., 1999) resulted in approximately a twofold increase in the strength of interaction with PP1 $\alpha$  (Fig. 2*a*). Thus, presence of the RIGL motif does not explain PP1 $\alpha$  specificity for the IC1 bait. Interestingly, the V1 variable region of IC1 bait alone

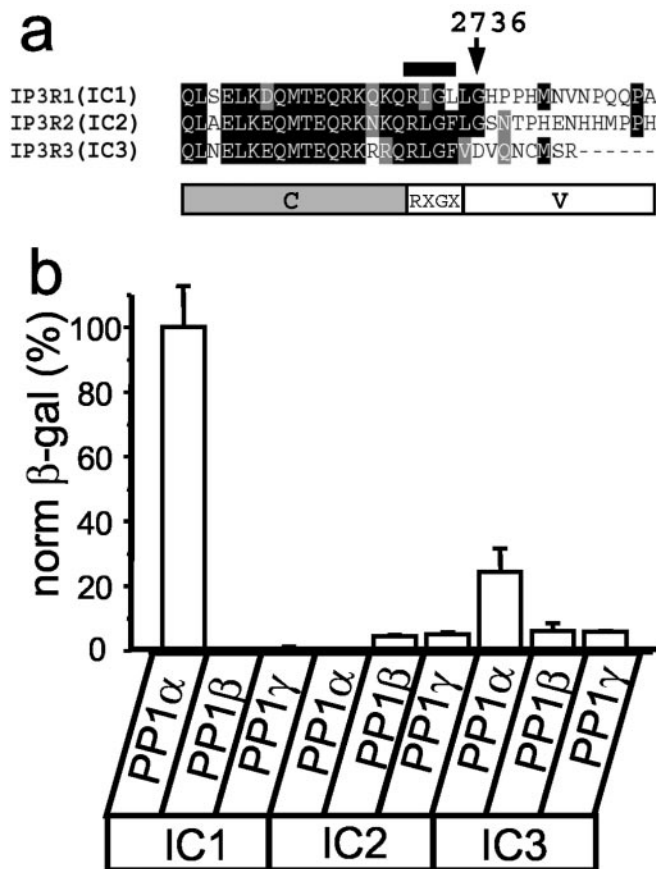


**Figure 1.** InsP<sub>3</sub>R1 specifically binds PP1 $\alpha$  in a yeast two-hybrid assay. *a*, Alignment of C-terminal regions of the InsP<sub>3</sub>R1, InsP<sub>3</sub>R2, and InsP<sub>3</sub>R3. The IC1 fragment was used as a bait in the yeast two-hybrid screen. The position of the <sup>2731</sup>RIGL<sup>2734</sup> motif in the IC1 bait is indicated by a bar above the sequence. The domain structure of the InsP<sub>3</sub>R C-terminal region [constant (C)-RXGX-variable (V)] is shown below the alignment. *b*, Specificity of InsP<sub>3</sub>R-PP1 interactions. IC1, IC2, and IC3 baits were tested for the strength of interactions with PP1 $\alpha$ , PP1 $\beta$ , and PP1 $\gamma$  preys in liquid yeast two-hybrid assays. The data are normalized to the strength of interaction for the IC1-PP1 $\alpha$  pair and are shown as mean  $\pm$  SEM ( $n \geq 3$ ).  $\beta$ -gal,  $\beta$ -galactosidase.

is not sufficient for association with PP1 $\alpha$  (Fig. 2*a*). From these results, we concluded that the association with PP1 $\alpha$  requires the RIGL motif and V1 variable region of IC1 (RIGL-V1, R2731-A2749), with the specificity for IC1 conferred by the variable region. To further confirm these findings, we coupled the peptides corresponding to the RXGX motif and variable sequence of InsP<sub>3</sub>R1, InsP<sub>3</sub>R2, and InsP<sub>3</sub>R3 to NHS-Sepharose and performed pull-down experiments with HA-tagged PP1 $\alpha$  transiently expressed in COS cells (Fig. 3*b*). We found that the InsP<sub>3</sub>R1-specific peptide (RIGL-V1) but not the InsP<sub>3</sub>R2- or the InsP<sub>3</sub>R3-specific peptides (RLGF-V2 and RLGF-V3) formed a salt-sensitive complex with HA-PP1 $\alpha$  (Fig. 2*b*).

To further confirm a specific association between InsP<sub>3</sub>R1 and PP1 $\alpha$ , we performed a series of *in vitro* binding experiments. For these experiments, full-length (RT1) and truncated (RT1 $\Delta$ C) rat InsP<sub>3</sub>R1 were expressed in insect cells by baculovirus infection (Fig. 3*a*) and solubilized in CHAPS. The HA-tagged PP1 $\alpha$ , PP1 $\beta$ , and PP1 $\gamma$  were transiently expressed in COS cells (Fig. 3*b*), solubilized in CHAPS, mixed with the InsP<sub>3</sub>R1-containing lysates, and precipitated with anti-HA antibodies. The amount of immunoprecipitated InsP<sub>3</sub>R1 was quantified by [<sup>3</sup>H]InsP<sub>3</sub> binding assay. We found that HA-PP1 $\alpha$ , but not HA-PP1 $\beta$  or HA-PP1 $\gamma$ , efficiently precipitated the InsP<sub>3</sub>R1 (Fig. 3*d*). The ability of HA-

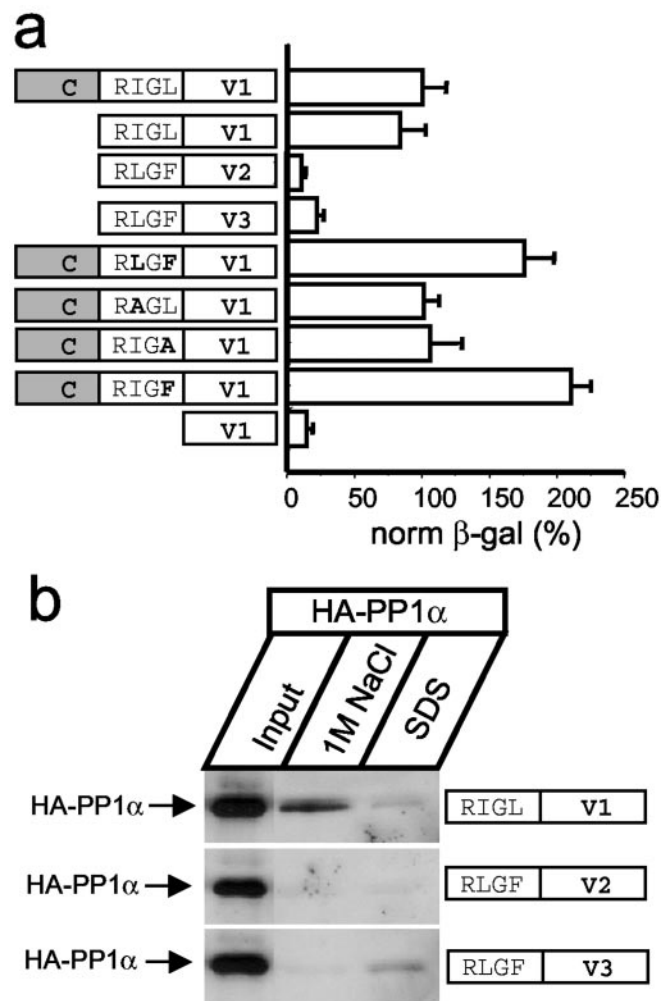


**Figure 2.** PP1 $\alpha$ -binding motif in the InsP<sub>3</sub>R1 sequence. *a*, Analysis of PP1 $\alpha$  binding specificity. IC1 (C-RIGL-V1, 2714–2749 of InsP<sub>3</sub>R1), RIGL-V1 (2731–2749 of InsP<sub>3</sub>R1), RLGF-V2 (2683–2701 of InsP<sub>3</sub>R2), RLGF-V3 (2658–2670 of InsP<sub>3</sub>R3), IC1 point mutants in the RIGL motif (indicated in bold), and V1 (2736–2749 of InsP<sub>3</sub>R1) baits were tested with PP1 $\alpha$  prey in liquid yeast two-hybrid assays. The data are normalized to the strength of interaction for the IC1-PP1 $\alpha$  pair and are shown as mean  $\pm$  SEM ( $n \geq 3$ ).  $\beta$ -gal,  $\beta$ -galactosidase. *b*, HA-PP1 $\alpha$  pull-down experiments with RIGL-V1 (2731–2749 of InsP<sub>3</sub>R1), RLGF-V2 (2683–2701 of InsP<sub>3</sub>R2), and RLGF-V3 (2658–2670 of InsP<sub>3</sub>R3) peptides. Fractions eluted from the beads by 1 M NaCl and SDS were analyzed by Western blotting with anti-HA mAbs. The input lane on all three panels contains 1/50th of the COS cell lysate used for pull-downs.

PP1 $\alpha$  to precipitate InsP<sub>3</sub>R1 critically depended on the InsP<sub>3</sub>R1 C-terminal region, because HA-PP1 $\alpha$  did not precipitate RT1 $\Delta$ C protein (Fig. 3*d*). In complementary experiments, we found that GST-IC1, but not GST alone, GST-IC2, or GST-IC3 proteins (Fig. 3*c*), effectively interfered with the InsP<sub>3</sub>R1 precipitation by HA-PP1 $\alpha$  (Fig. 3*d*). Thus, the most C-terminal region of the InsP<sub>3</sub>R1 is both necessary and sufficient for specific association with PP1 $\alpha$ .

Do InsP<sub>3</sub>R1 and PP1 $\alpha$  associate *in vivo*? In the brain, PP1 $\alpha$  is concentrated in postsynaptic spines (Ouimet et al., 1995). The InsP<sub>3</sub>R1 is also present in postsynaptic terminals (Sharp et al., 1993a,b). To establish whether InsP<sub>3</sub>R1-PP1 $\alpha$  complexes form in synaptic locations, we isolated cortical rat brain synaptosomes, extracted the obtained material in CHAPS, precipitated with the anti-InsP<sub>3</sub>R1 polyclonal antibody, and blotted with the anti-PP1 mAb. We found that PP1 was precipitated by anti-InsP<sub>3</sub>R1 antibodies but not by the preimmune sera (Fig. 4*a*). In the brain, the

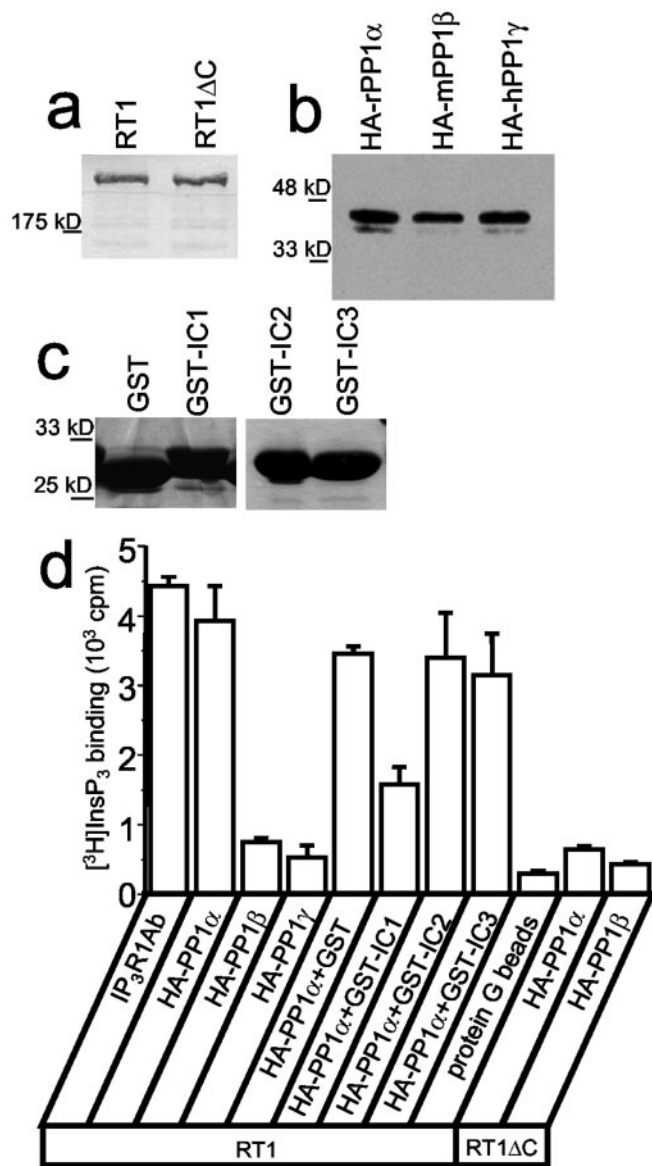


**Figure 3.** InsP<sub>3</sub>R1 binds PP1 $\alpha$  *in vitro*. *a*, Expression of full-length (RT1) or truncated (RT1 $\Delta$ C) recombinant InsP<sub>3</sub>R1 in Sf9 cells was analyzed by Western blotting with polyclonal antibodies directed against the InsP<sub>3</sub>R1 N-terminal region (cycl3b2). *b*, Expression of HA-tagged  $\alpha$ ,  $\beta$ , and  $\gamma$  PP1 isoforms in COS cells was analyzed by Western blotting with anti-HA mAbs. *c*, GST, GST-IC1, GST-IC2, and GST-IC3 proteins were expressed in BL21 *Escherichia coli* was purified on glutathione beads and analyzed by Coomassie staining. *d*, Analysis of InsP<sub>3</sub>R1–PP1 association *in vitro* by immunoprecipitation. HA-tagged  $\alpha$ ,  $\beta$ , and  $\gamma$  PP1 isoforms were mixed with solubilized full-length (RT1) or truncated (RT1 $\Delta$ C) recombinant InsP<sub>3</sub>R1 and precipitated with anti-HA mAbs. GST, GST-IC1, GST-IC2, and GST-IC3 proteins were included in the immunoprecipitation reactions at a 200  $\mu$ g/ml concentration as indicated. The amount of precipitated InsP<sub>3</sub>R1 was quantified by [<sup>3</sup>H]InsP<sub>3</sub> binding. Anti-InsP<sub>3</sub>R1 mAbs (IP<sub>3</sub>R1Ab) were used as a positive control; empty beads (protein G beads) were used as a negative control.

PP1 $\alpha$  isoform is most enriched in the neostriatum region (da Cruz e Silva et al., 1995). Are InsP<sub>3</sub>R1–PP1 $\alpha$  complexes formed in the neostriatum? By following published procedures (Nishi et al., 1997), we isolated the neostriatum region of the adult rat brain and performed immunoprecipitation experiments. Similar to experiments with the synaptosomes, PP1 was precipitated from the neostriatum by anti-InsP<sub>3</sub>R1 antibodies but not by the preimmune sera (Fig. 4*b*). Thus, InsP<sub>3</sub>R1–PP1 complexes exist in synaptic locations and in the neostriatum region of the brain. The PP1 mAbs available to us do not discriminate between different

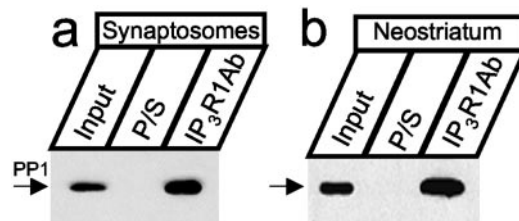


**Figure 4.** InsP<sub>3</sub>R1 binds PP1 $\alpha$  *in vivo*. The InsP<sub>3</sub>R1 forms complexes with PP1 in brain synaptosomes (*a*) and in the neostriatum (*b*). The samples were precipitated with anti-InsP<sub>3</sub>R1 polyclonal antibodies (T443) and blotted with anti-PP1 mAbs. Preimmune sera (P/S) were used as a negative control. The input lane on *a* and *b* contains 1/50th of the lysate used for immunoprecipitation. Quantification of PP1 band intensity suggests that 3.8% (synaptosomes) and 3.4% (neostriatum) of total PP1 is associated with the InsP<sub>3</sub>R1.

PP1 isoforms, but based on the specificity of InsP<sub>3</sub>R1 interactions *in vitro* (Figs. 1–3), it is likely that the observed complexes correspond to InsP<sub>3</sub>R1–PP1 $\alpha$ .

#### PP1 $\alpha$ dephosphorylates PKA-phosphorylated InsP<sub>3</sub>R1 *in vitro*

The InsP<sub>3</sub>R1 is one of the major substrates of PKA phosphorylation in the brain (Supattapone et al., 1988; Danoff et al., 1991; Ferris et al., 1991a; Haug et al., 1999; Pieper et al., 2001). In the neostriatum, PP1 and PKA play an antagonistic role (Greengard et al., 1999). Can neostriatal PP1 dephosphorylate InsP<sub>3</sub>R1? To answer this question, we performed a series of *in vitro* dephosphorylation experiments. For these experiments, InsP<sub>3</sub>R1 (RT1) was expressed in insect cells by baculovirus infection (Fig. 3*a*), immunoprecipitated, and phosphorylated *in vitro* by a catalytic subunit of PKA in the presence of [ $\gamma$ -<sup>32</sup>P]ATP. The <sup>32</sup>P-InsP<sub>3</sub>R1 was incubated for a variable amount of time with the rat neostriatal homogenate. Rapid dephosphorylation of <sup>32</sup>P-InsP<sub>3</sub>R1 by neostriatal homogenate was observed (Fig. 5*a*). The dephosphorylation assay was performed in the presence of 0.1 mM EGTA and 1 nM okadaic acid to inhibit PP2A, PP2B, and PP2C activities (Nishi et al., 1999). Under these conditions, dephosphorylation of InsP<sub>3</sub>R1 by neostriatal homogenate was almost completely inhibited by Inh2 (Fig. 5*c*), confirming that the observed phosphatase activity corresponds to the activity of endogenous nsPP1.

The substrate specificity of PP1 is primarily determined by its targeting subunits, such as spinophilin, neurabin, and G<sub>M</sub> (Greengard et al., 1999). Is it possible that the identified InsP<sub>3</sub>R1–PP1 $\alpha$  association (Figs. 1–4) facilitates the InsP<sub>3</sub>R1 dephosphorylation by PP1? To test this hypothesis, we compared the rates of <sup>32</sup>P-InsP<sub>3</sub>R1 dephosphorylation by nsPP1 in the presence of GST and GST-IC1 proteins (Fig. 3*c*). We found that dephosphorylation of <sup>32</sup>P-InsP<sub>3</sub>R1 by nsPP1 was significantly faster in the presence of GST than in the presence of GST-IC1 (Fig. 5*a*). To quantify these data, the content of the <sup>32</sup>P-InsP<sub>3</sub>R1 band at each time point was quantified by phosphoimaging (Fig. 5*a*) and normalized to time 0. When the normalized <sup>32</sup>P-InsP<sub>3</sub>R1 content was plotted versus time of incubation with nsPP1 in semilogarithmic coordinates, the measured values could be fitted by the straight line (Fig. 5*b*), the slope of which corresponds to the rate of the <sup>32</sup>P-InsP<sub>3</sub>R1 dephosphorylation. On average, for our experimental conditions the nsPP1 dephosphorylated <sup>32</sup>P-InsP<sub>3</sub>R1 at a rate of  $0.13 \pm 0.02$  ( $n = 3$ ) min<sup>-1</sup> in the presence of GST and at a rate of  $0.054 \pm 0.006$  ( $n = 3$ ) min<sup>-1</sup> in the presence of GST-IC1 (Fig. 5*c*).

To further analyze the specificity of InsP<sub>3</sub>R1 dephosphorylation by PP1, we performed a series of *in vitro* dephosphorylation experiments with recombinant PP1. Similar to results with en-

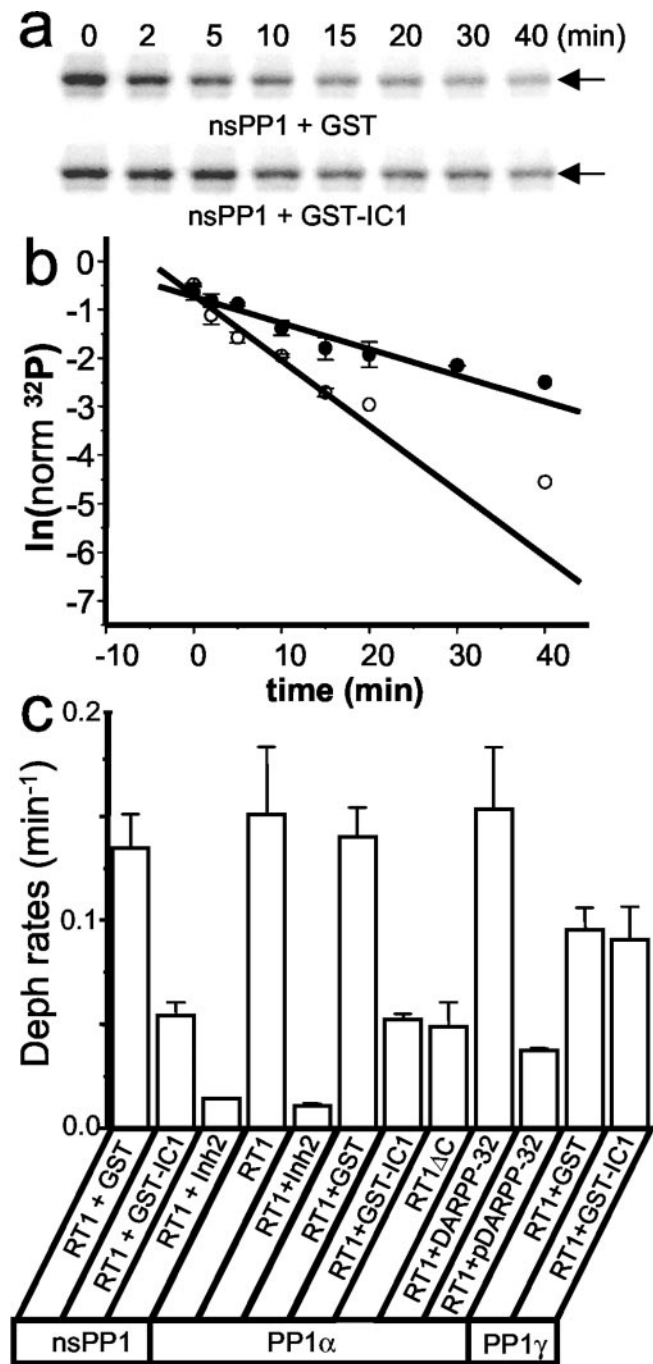


**Figure 5.** PP1 dephosphorylates the InsP<sub>3</sub>R1 *in vitro*. *a*, Effects of GST (*top*) and GST-IC1 (*bottom*) on the <sup>32</sup>P-InsP<sub>3</sub>R1 dephosphorylation by endogenous nsPP1 *in vitro*. For each sample, the time of incubation with nsPP1 is indicated above the autoradiogram. The experiment was repeated three times with similar results. *b*, The normalized data from several independent experiments were averaged together and plotted in semilogarithmic coordinates as mean  $\pm$  SE ( $n = 3$ ) for experiments in the presence of GST (*open circles*) and GST-IC1 (*filled circles*). The rate of the dephosphorylation reaction is determined from the slope of the *straight line* used to fit the data. *c*, Summary of the <sup>32</sup>P-InsP<sub>3</sub>R1 *in vitro* dephosphorylation experiments. The rates of <sup>32</sup>P-InsP<sub>3</sub>R1 dephosphorylation (*Deph*) reactions determined as described for *b* are shown as mean  $\pm$  SE ( $n \geq 3$ ). DARPP-32 and pDARPP-32 indicate recombinant unphosphorylated and PKA-phosphorylated forms of DARPP-32, respectively.

ogenous nsPP1, we found that recombinant PP1 $\alpha$  rapidly dephosphorylates <sup>32</sup>P-InsP<sub>3</sub>R1 (Fig. 5c). As with nsPP1, dephosphorylation of <sup>32</sup>P-InsP<sub>3</sub>R1 by PP1 $\alpha$  was abolished by PP1 inhibitor 2 (Fig. 5c). Similar to nsPP1, we observed a threefold

reduction in the rate of <sup>32</sup>P-InsP<sub>3</sub>R1 dephosphorylation by PP1 $\alpha$  in the presence of GST-IC1 but not in the presence of GST (Fig. 5c). A similar effect was caused by truncation of the InsP<sub>3</sub>R1 C-terminal in RT1 $\Delta$ C mutant (Fig. 5c). Similar to PP1 $\alpha$ , the PP1 $\gamma$  isoform was also able to dephosphorylate <sup>32</sup>P-InsP<sub>3</sub>R1 *in vitro* (Fig. 5c). The absolute rates of PP1 $\alpha$ - and PP1 $\gamma$ -mediated dephosphorylation of <sup>32</sup>P-InsP<sub>3</sub>R1 are not comparable, because different amounts of phosphatase activity were added to the dephosphorylation reactions. Importantly, in contrast to experiments with PP1 $\alpha$ , GST-IC1 had no effect on the rate of <sup>32</sup>P-InsP<sub>3</sub>R1 dephosphorylation by PP1 $\gamma$  (Fig. 5c). This result agrees with the inability of InsP<sub>3</sub>R1 and PP1 $\gamma$  to form a complex in yeast two-hybrid and biochemical assays (Figs. 1*b*, 3*d*). From the results shown on Figure 5c, we concluded that direct association of PP1 $\alpha$  with the InsP<sub>3</sub>R1 C-terminal enables efficient dephosphorylation of <sup>32</sup>P-InsP<sub>3</sub>R1 by PP1 $\alpha$ . In the neostriatum, DARPP-32 plays a predominant role in control of PP1 activity (Greengard et al., 1999). We found that the PKA-phosphorylated form pDARPP-32, but not DARPP-32 itself, inhibited <sup>32</sup>P-InsP<sub>3</sub>R1 dephosphorylation by PP1 $\alpha$  (Fig. 5c).

#### PKA phosphorylation of neostriatal InsP<sub>3</sub>R1 *in vivo*

In the neostriatum, stimulation of D1 dopamine receptors causes an increase in cAMP levels (Greengard et al., 1999). Are neostriatal InsP<sub>3</sub>R1s phosphorylated by PKA when cAMP is elevated? To answer this question, we used the PKA back-phosphorylation method to determine the fraction of neostriatal InsP<sub>3</sub>R1 in the phosphorylated state (pInsP<sub>3</sub>R1). By following published procedures (Nishi et al., 1997), we isolated neostriatal slices from adult rat brains and incubated them in the oxygenated Krebs media. For back-phosphorylation experiments, the neostriatal InsP<sub>3</sub>R1 was solubilized in CHAPS in the presence of phosphatase inhibitors, immunoprecipitated with anti-InsP<sub>3</sub>R1 antibodies, phosphorylated *in vitro* by the catalytic subunit of PKA in the presence of [ $\gamma$ -<sup>32</sup>P]ATP, separated by electrophoresis, and analyzed by phosphoimaging. When the sample was incubated with PP1 $\alpha$  before *in vitro* phosphorylation by PKA, the content of the <sup>32</sup>P-InsP<sub>3</sub>R1 band was the greatest (Fig. 6*a*, PP1 $\alpha$  lane). This value was interpreted as total InsP<sub>3</sub>R1 in the neostriatal sample (<sup>32</sup>P<sub>PP1 $\alpha$</sub> ). Without preincubation with PP1 $\alpha$ , the content of the <sup>32</sup>P-InsP<sub>3</sub>R1 band was reduced by  $\sim$ 30% (Fig. 6*a*, *Ctrl* lane). By using the normalization procedure described in Materials and Methods, we determined that  $37 \pm 3\%$  ( $n = 4$ ) of InsP<sub>3</sub>R1s in the neostriatum are in the PKA-phosphorylated state in control conditions (Fig. 6*b*). When neostriatal slices were incubated with 1 mM 8-Br-cAMP or 100  $\mu$ M dopamine for 10 min, we observed a drastic reduction in the content of the <sup>32</sup>P-InsP<sub>3</sub>R1 band (Fig. 6*a*, *cAMP* and *Dop* lanes). We estimated that 8-Br-cAMP and dopamine increased the fraction of PKA-phosphorylated InsP<sub>3</sub>R1 in the neostriatum to  $86 \pm 6\%$  ( $n = 4$ ) and  $85 \pm 8\%$  ( $n = 4$ ), respectively (Fig. 6*b*). Preincubation of neostriatal slices for 60 min with 5  $\mu$ M cyclosporine A, a calcineurin inhibitor, or 400  $\mu$ M calyculin A, a PP1/PP2A inhibitor, increased the fraction of PKA-phosphorylated InsP<sub>3</sub>R1 to  $71 \pm 4\%$  ( $n = 4$ ) and  $68 \pm 3\%$  ( $n = 4$ ), respectively (Fig. 6*a,b*, *CsA* and *CalA* lanes). In contrast, preincubation of neostriatal slices with 10 nM okadaic acid, a specific inhibitor of PP2A at this concentration, had only a minor effect on the PKA-phosphorylated state of InsP<sub>3</sub>R1 when compared with control conditions (Fig. 6*a,b*, *OA* lane).

To determine a dynamic of dopamine-induced InsP<sub>3</sub>R1 phos-

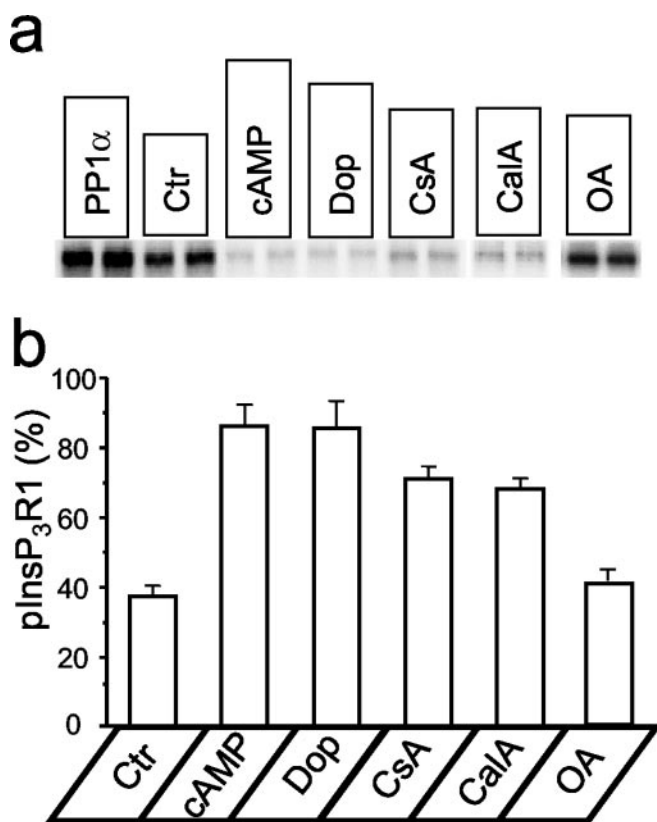


**Figure 6.** PKA phosphorylation of neostriatal InsP<sub>3</sub>R1 *in vivo*. PKA back-phosphorylation of neostriatal InsP<sub>3</sub>R1 after pretreatment with PP1 $\alpha$  (PP1 $\alpha$ ); in controls (Ctr); after 10 min of incubation of neostriatal slices with 1 mM 8-Br-cAMP (cAMP) or 100  $\mu$ M dopamine (Dop); or after 60 min of treatment with 5  $\mu$ M cyclosporine A (CsA), 400  $\mu$ M calyculin A (CalA), or 10 nM okadaic acid (OA). *a*, Autoradiogram of a representative experiment. The data for calyculin A and okadaic acid are taken from the different experiments. *b*, Summary of neostriatal InsP<sub>3</sub>R1 back-phosphorylation experiments. The estimated fraction of PKA-phosphorylated InsP<sub>3</sub>R1 in neostriatal slices (see Materials and Methods) is shown as mean  $\pm$  SE ( $n = 4$ ).

phorylation in the neostriatal slices, we used the PKA back-phosphorylation method at different time points after application of 100  $\mu$ M dopamine. We found that the fraction of PKA-phosphorylated InsP<sub>3</sub>R1 peaks 10–15 min after dopamine application and returns to prestimulation levels within 30 min (Fig. 7*a*). Thus, similar to DARPP-32 (Nishi et al., 1997; Greengard et al., 1999), the dopamine-induced phosphorylation of neostriatal InsP<sub>3</sub>R1 by PKA is transient, although with a slower time course. The dopamine-induced changes in the InsP<sub>3</sub>R1

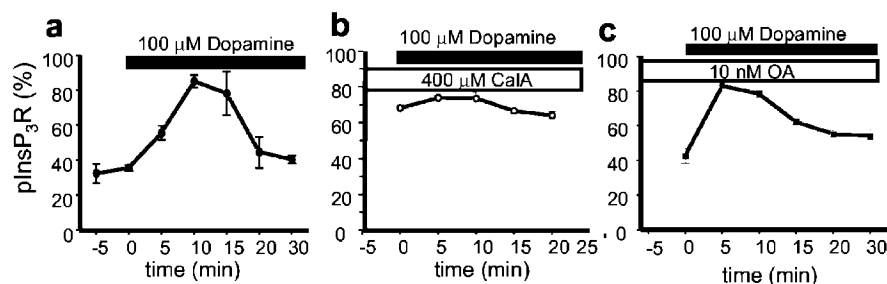


**Figure 7.** Dopamine induces transient phosphorylation of neostriatal InsP<sub>3</sub>R1 by PKA. *a*, Time course of changes in neostriatal InsP<sub>3</sub>R1 PKA-phosphorylated state in response to application of 100  $\mu$ M dopamine. Dopamine was applied to neostriatal slices at time 0. At each time point, the fraction of neostriatal InsP<sub>3</sub>R1 in the PKA-phosphorylated state is shown as mean  $\pm$  SE ( $n = 3$ ) (filled circles). *b*, *c*, The same experiment as in *a* performed with slices exposed to 400  $\mu$ M calyculin A (CalA, *b*) (open circles) or 10 nM okadaic acid (OA, *c*) (filled squares) for 60 min before the application of dopamine.

phosphorylated state were abolished by preincubation of neostriatal slices with 400  $\mu$ M calyculin A, a PP1/PP2A inhibitor (Fig. 7*b*). In contrast, preincubation of neostriatal slices with 10 nM okadaic acid, a specific inhibitor of PP2A at this concentration, had only a minimal effect on dopamine-induced changes in neostriatal InsP<sub>3</sub>R1 phosphorylated state (Fig. 7*c*). From the obtained pharmacological profile (Figs. 6, 7), we concluded that the PKA-phosphorylated state of neostriatal InsP<sub>3</sub>R1 in the resting state and in response to stimulation with dopamine is determined by the activity of PP1 and PP2B phosphatases but not by the activity of PP2A phosphatase.

### PKA activates and PP1 $\alpha$ inhibits InsP<sub>3</sub>R1

What are the functional consequences of InsP<sub>3</sub>R1 phosphorylation by PKA? Ca<sup>2+</sup> flux measurements used previously to address this question provided conflicting answers (Supattapone et al., 1988; Nakade et al., 1994; Cameron et al., 1995; Wojcikiewicz and Luo, 1998). To study modulation of the InsP<sub>3</sub>R1 by PKA phosphorylation, we incorporated recombinant InsP<sub>3</sub>R1 expressed in insect cells into planar lipid bilayers by microsomal fusion (Tu et al., 2002). Addition of 2  $\mu$ M InsP<sub>3</sub> to the cytosolic (*cis*) chamber induced InsP<sub>3</sub>R1 activity (Fig. 8*a*, second trace), but the  $P_o$  was only 5–10% (Fig. 8*b*). In the presence of 0.5 mM MgATP in the *cis* chamber, the application of PKA catalytic subunit directly to the bilayer induced immediate facilitation in channel activity (Fig. 8*a*, third trace), with a  $P_o$  of phosphorylated channels in the range of 30–40% (Fig. 8*b*). Application of PP1 $\alpha$  to the bilayer resulted in almost complete inhibition of channel activity (Fig. 8*a*, fourth trace, *b*). Inactivation of InsP<sub>3</sub>R1 by PP1 $\alpha$  could be reversed by a second application of PKA catalytic subunit (Fig. 8*a*, fifth trace, *b*), which in turn could be counteracted by the second application of PP1 $\alpha$  (Fig. 8*a*, sixth trace, *b*). Results similar to the experiment shown in Figure 8*a*, *b* were obtained in three independent experiments. No effect was observed if the catalytic subunit of PKA was boiled before addition to the bilayer ( $n = 5$ ) or if 0.5 mM Na<sub>2</sub>ATP was present in the *cis* chamber instead of MgATP ( $n = 3$ ). As an additional control, we performed experiments with a nonhydrolysable ATP analog, ATP $\gamma$ S. If 100  $\mu$ M Mg-ATP $\gamma$ S was present in the *cis* chamber, the application of a catalytic subunit of PKA to the bilayer resulted in InsP<sub>3</sub>R1 activation that could no longer be reversed by PP1 $\alpha$  or affected by a second application of PKA (Fig. 8*c*). From our experiments, we concluded that under identical experimental conditions PP1 $\alpha$ -dephosphorylated InsP<sub>3</sub>R1s have low  $P_o$  (<2–3%), and PKA-phosphorylated InsP<sub>3</sub>R1s have much higher  $P_o$  (30–40%).

To test the importance of InsP<sub>3</sub>R1–PP1 $\alpha$  association for InsP<sub>3</sub>R1 modulation by PKA phosphorylation, we performed planar lipid bilayer experiments with RT1 $\Delta$ C mutants expressed in Sf9 cells (Fig. 3*a*). We found that RT1 $\Delta$ C mutants formed functional InsP<sub>3</sub>-gated channels, which were modulated by PKA and PP1 $\alpha$  in a manner similar to the wild-type InsP<sub>3</sub>R1 (data not shown). To explain these results, we reasoned that because of the high concentration of PP1 $\alpha$  added to the bilayer, the C-terminal PP1 $\alpha$ -docking site in the InsP<sub>3</sub>R1 sequence is not important for functional regulation of InsP<sub>3</sub>R1 in our *in vitro* experiments. However, *in*

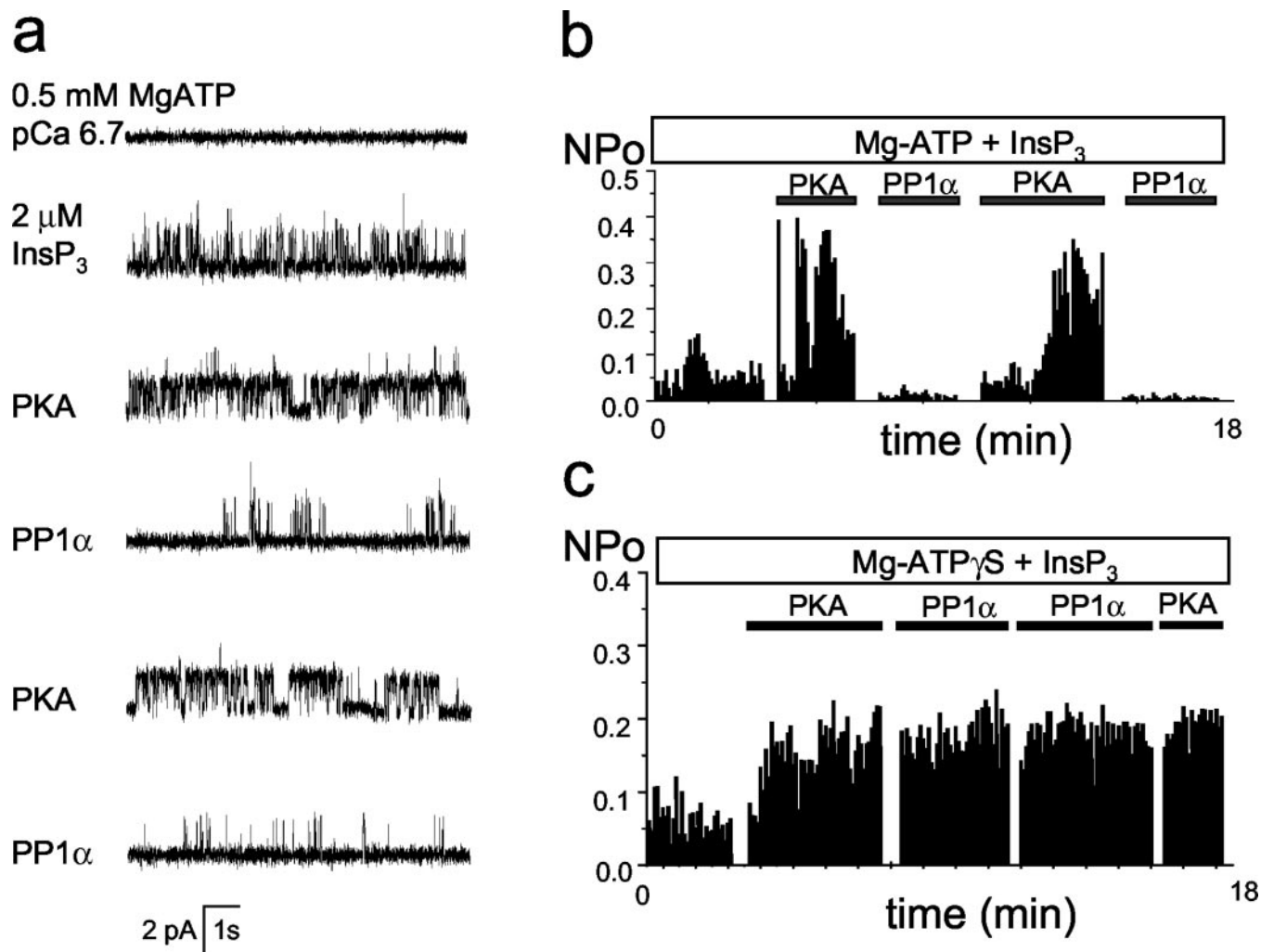


**Figure 8.** PKA and PP1 $\alpha$  modulate InsP<sub>3</sub>R1 activity in planar lipid bilayers. *a*, PKA activates and PP1 $\alpha$  inhibits the recombinant InsP<sub>3</sub>R1 reconstituted into planar lipid bilayers. Each trace corresponds to 10 sec of current recordings from the same experiment. The experiment is performed in the presence of pCa 6.7 and 0.5 mM Mg-ATP in the *cis* chamber. Additions of 2  $\mu$ M InsP<sub>3</sub> to the *cis* chamber and PKA/PP1 $\alpha$  directly to the bilayer are indicated. Similar results were obtained in three independent experiments. *b*, The average InsP<sub>3</sub>R1  $P_o$  is calculated for a 5 sec window of time and plotted for the duration of an experiment. The times of InsP<sub>3</sub>, PKA, and PP1 $\alpha$  additions are shown above the  $P_o$  plot. The same experiment was used to generate *a* and *b*. *c*, The InsP<sub>3</sub>R1  $P_o$  plot for the experiment performed in the presence of 100  $\mu$ M Mg-ATP $\gamma$ S in the *cis* chamber. The times of InsP<sub>3</sub>, PKA, and PP1 $\alpha$  additions are shown above the  $P_o$  plot. Similar results were obtained in three independent experiments.

*in vivo* the concentration of PP1 $\alpha$  is much lower, and InsP<sub>3</sub>R1–PP1 $\alpha$  association is likely to play an important role in control of the InsP<sub>3</sub>R1 PKA-phosphorylated state.

#### Mechanism of InsP<sub>3</sub>R1 activation by PKA

To obtain mechanistic insights into InsP<sub>3</sub>R1 activation by PKA, we evaluated effects of PKA phosphorylation on Ca<sup>2+</sup> and InsP<sub>3</sub> dependence of recombinant InsP<sub>3</sub>R1 reconstituted into planar lipid bilayers. In the first series of experiments, the activity of InsP<sub>3</sub>R1 was recorded at variable Ca<sup>2+</sup> concentrations in the presence of 2  $\mu$ M InsP<sub>3</sub> and 0.5 mM Mg-ATP. With addition of InsP<sub>3</sub>, we observed two distinct populations of InsP<sub>3</sub>R1. In some (6 of 14) experiments, the initial activity of InsP<sub>3</sub>R1 was low, with  $P_o \leq 10\%$  (“low-activity” channels). In other experiments (8 of 14), the activity of InsP<sub>3</sub>R1 was much higher, with  $P_o \sim 30\%$  (“high-activity” channels). As described in the previous section, addition of PKA to low-activity channels increased their  $P_o$  to 30–40% (Fig. 8). Addition of PKA to high-activity channels had very little or no effect on their  $P_o$ , but addition of PP1 $\alpha$  reduced their  $P_o$  to levels of <10% (data not shown). In *in vitro* back-

phosphorylation experiments, we determined that  $\sim 20\%$  of recombinant InsP<sub>3</sub>R1 in microsomes isolated from Sf9 cells are in the PKA-phosphorylated state (data not shown), presumably because of activity of endogenous PKA present in Sf9 cells. Thus, we reasoned that high-activity channels are likely to correspond to partially phosphorylated InsP<sub>3</sub>R1, and low-activity channels correspond to unphosphorylated InsP<sub>3</sub>R1.

The experiments in the previous section (Fig. 8) were performed with low-activity channels. In Ca<sup>2+</sup>-dependence experiments, we compared the behavior of low-activity, high-activity, and PKA-phosphorylated channels. In agreement with our previous findings (Nosyreva et al., 2002; Tu et al., 2002), recombinant high-activity InsP<sub>3</sub>R1 displayed bell-shaped dependence on cytosolic Ca<sup>2+</sup> with the peak at pCa 6.65 (Fig. 9, *open circles*). The parameters of the optimal fit ( $P_m$ ,  $n$ ,  $k$ ,  $K$ ) for each series of Ca<sup>2+</sup>-dependence experiments are presented in Table 1. Fit to the data using the modified bell-shaped equation (see Materials and Methods) yielded the affinity of activating site equal to 0.22  $\mu$ M Ca<sup>2+</sup>, the affinity of inhibitory site equal to 0.21  $\mu$ M Ca<sup>2+</sup>, and the cooperativity coefficient of 1.31 (Fig. 9, *smooth curve*;

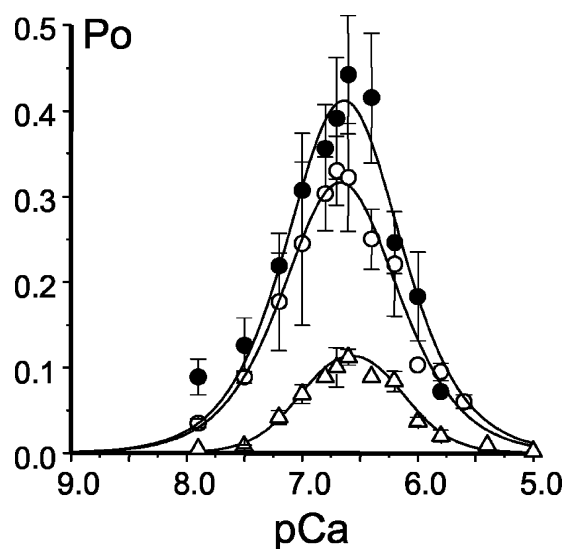


**Figure 9.** Effect of PKA on InsP<sub>3</sub>R1 Ca<sup>2+</sup> dependence. The  $P_o$  of recombinant InsP<sub>3</sub>R1 was determined in the presence of 2  $\mu$ M InsP<sub>3</sub> and 0.5 mM MgATP at *cis* (cytosolic) Ca<sup>2+</sup> concentrations in the range between 10 nM and 5  $\mu$ M Ca<sup>2+</sup>.  $P_o$  values measured in several independent experiments were averaged together at each Ca<sup>2+</sup> concentration as described in Materials and Methods and shown as mean  $\pm$  SE for low-activity InsP<sub>3</sub>R1 ( $n = 2$ ; open triangles), high-activity InsP<sub>3</sub>R1 ( $n = 3$ ; open circles), and PKA-phosphorylated InsP<sub>3</sub>R1 ( $n = 3$ ; filled circles). The averaged data were fitted by the bell-shaped equation modified from Bezprozvanny et al. (1991), as explained in Materials and Methods. The parameters of the optimal fits (smooth curves) are shown in Table 1.

Table 1). Recombinant low-activity InsP<sub>3</sub>R1 displayed similar bell-shaped Ca<sup>2+</sup> dependence with the peak at pCa 6.55 (Fig. 9, open triangles). Fit to low-activity data set yielded the affinity of activating site equal to 0.10  $\mu$ M Ca<sup>2+</sup>, the affinity of inhibitory site equal to 0.72  $\mu$ M Ca<sup>2+</sup>, and the cooperativity coefficient of 2.09 (Fig. 9, smooth curve; Table 1). When the same experiment was performed with the InsP<sub>3</sub>R1 phosphorylated by PKA in bilayers (initially displaying low activity), we found that the PKA-phosphorylated InsP<sub>3</sub>R1 also displayed bell-shaped Ca<sup>2+</sup> dependence that peaked at pCa 6.65 (Fig. 9, filled circles). For PKA-phosphorylated InsP<sub>3</sub>R1, the fit yielded the affinity of activating site equal to 0.24  $\mu$ M Ca<sup>2+</sup>, the affinity of inhibitory site equal to 0.21  $\mu$ M Ca<sup>2+</sup>, and the cooperativity coefficient of 1.32 (Fig. 9, smooth curve; Table 1). From these experiments, we concluded that PKA phosphorylation induces only minor changes in bell-shaped Ca<sup>2+</sup> dependence of the InsP<sub>3</sub>R1.

In the next series of experiments, we analyzed effects of PKA on InsP<sub>3</sub> dependence of InsP<sub>3</sub>R1. These experiments were performed in the presence of 300 nM Ca<sup>2+</sup> (pCa 6.7) and 0.5 mM MgATP on the cytosolic side of the bilayer. By adding increasing amounts of InsP<sub>3</sub> to the *cis* chamber, we determined that the apparent affinity of high-activity InsP<sub>3</sub>R1 for InsP<sub>3</sub> ( $k_{\text{InsP}_3}$ ) is equal to 0.19  $\mu$ M InsP<sub>3</sub> (Fig. 10a, open circles). The apparent af-

finity of low-activity InsP<sub>3</sub>R1 could not be reliably determined because of the extremely low  $P_o$  of these channels at low InsP<sub>3</sub> concentrations (data not shown). To determine the effect of PKA on the InsP<sub>3</sub> dependence of InsP<sub>3</sub>R1, we started an experiment by addition of 100 nM InsP<sub>3</sub>. The InsP<sub>3</sub>R1 activity at this concentration of InsP<sub>3</sub> was very low (Fig. 10b, second trace), with a  $P_o$  of 1–2% (Fig. 10c). Addition of PKA to the bilayer resulted in dramatic activation of InsP<sub>3</sub>R1 (Fig. 10b, third trace), with the  $P_o$  increased to 30–40% (Fig. 10c). Increasing the InsP<sub>3</sub> concentration from 100 nM to 2  $\mu$ M did not result in additional InsP<sub>3</sub>R1 activation (Fig. 10b, traces 4–6, and c). Thus, PKA-phosphorylated InsP<sub>3</sub>R1s are maximally activated by 100 nM InsP<sub>3</sub>, indicating that the  $k_{\text{InsP}_3}$  value for PKA-phosphorylated InsP<sub>3</sub>R1 must be <50 nM InsP<sub>3</sub>. This estimate is in contrast to the values measured for high-activity InsP<sub>3</sub>R1 in the absence of PKA treatment (Fig. 10a). From these experiments, we concluded that PKA phosphorylation causes at least a fourfold increase in InsP<sub>3</sub>R1 sensitivity to activation by InsP<sub>3</sub>.

## Discussion

Modulation of InsP<sub>3</sub>R1 by PKA and PP1 $\alpha$  was investigated in this study. The main conclusions of our study are as follows: (1) the InsP<sub>3</sub>R1 specifically associates with PP1 $\alpha$  via the C-terminal region; (2) association with PP1 $\alpha$  facilitates dephosphorylation of PKA-phosphorylated InsP<sub>3</sub>R1; (3) the neostriatal InsP<sub>3</sub>R1s are phosphorylated by PKA after exposure of neostriatal slices to 8-Br-cAMP, cyclosporine A, calyculin A, but not to 10 nM okadaic acid; (4) the neostriatal InsP<sub>3</sub>R1s are transiently phosphorylated by PKA after application of dopamine; (5) the dopamine-induced PKA phosphorylation of neostriatal InsP<sub>3</sub>R1 is affected by cyclosporine A but not by 10 nM okadaic acid; (6) the InsP<sub>3</sub>R1s reconstituted into planar lipid bilayers are activated by PKA and inhibited by PP1 $\alpha$ ; (7) phosphorylation of InsP<sub>3</sub>R1 by PKA does not shift the peak of InsP<sub>3</sub>R1 bell-shaped Ca<sup>2+</sup> dependence; (8) phosphorylation of InsP<sub>3</sub>R1 by PKA induces at least a fourfold increase in the sensitivity of InsP<sub>3</sub>R1 to activation by InsP<sub>3</sub>. Implications of these findings for InsP<sub>3</sub>R1 function and dopaminergic signaling in the neostriatum are briefly discussed below.

### Modulation of InsP<sub>3</sub>R1 activity by PKA

A number of previous biochemical studies analyzed phosphorylation of InsP<sub>3</sub>R1 by PKA. The neuronal InsP<sub>3</sub>R1 is one of the best-known substrates for both endogenous and exogenous PKA (Walaas et al., 1986; Supattapone et al., 1988; Maeda et al., 1990; Danoff et al., 1991; Ferris et al., 1991b; Wojcikiewicz and Luo, 1998; Haug et al., 1999; Pieper et al., 2001). Two putative PKA phosphorylation sites (S1756 and S1589) are present in the coupling domain of the InsP<sub>3</sub>R1 (Danoff et al., 1991; Ferris et al., 1991a; Haug et al., 1999). In the cerebellum, Ser-1756 is the primary site of phosphorylation by PKA, whereas much higher PKA activity is required to phosphorylate Ser-1589 (Ferris et al., 1991b; but see Haug et al., 1999). Interestingly, the region of InsP<sub>3</sub>R1 between these two phosphorylation sites is alternatively spliced in a tissue-specific manner, with the stretch of 39 aa residues deleted in the non-neuronal isoform of the receptor (Danoff et al., 1991). This splicing event appears to change the pattern of phosphorylation by PKA, because InsP<sub>3</sub>R1 purified from vas deferens (short, non-neuronal isoform) is phosphorylated by PKA almost exclusively on Ser-1589 (Danoff et al., 1991). Potentially, this difference may form a basis for a tissue-specific regulation of InsP<sub>3</sub>R1 function by cAMP-mediated signaling pathways.

Despite this wealth of biochemical information, the functional consequences of InsP<sub>3</sub>R1 phosphorylation by PKA are

**Table 1.** Parameters of the bell-shaped fit to the Ca<sup>2+</sup>-dependence data obtained with control (low and high activity) and PKA-phosphorylated InsP<sub>3</sub>R1

InsP <sub>3</sub> R1	$P_m$	Hill coefficient ( $n$ )	Affinity of the activating site $k$ ( $\mu$ M)	Affinity of the inhibitory site $K$ ( $\mu$ M)	Peak of Ca <sup>2+</sup> dependence (pCa)
Low activity	2.25	2.10	0.10	0.72	6.55
High activity	0.3	1.31	0.22	0.21	6.65
PKA	0.38	1.32	0.24	0.21	6.65

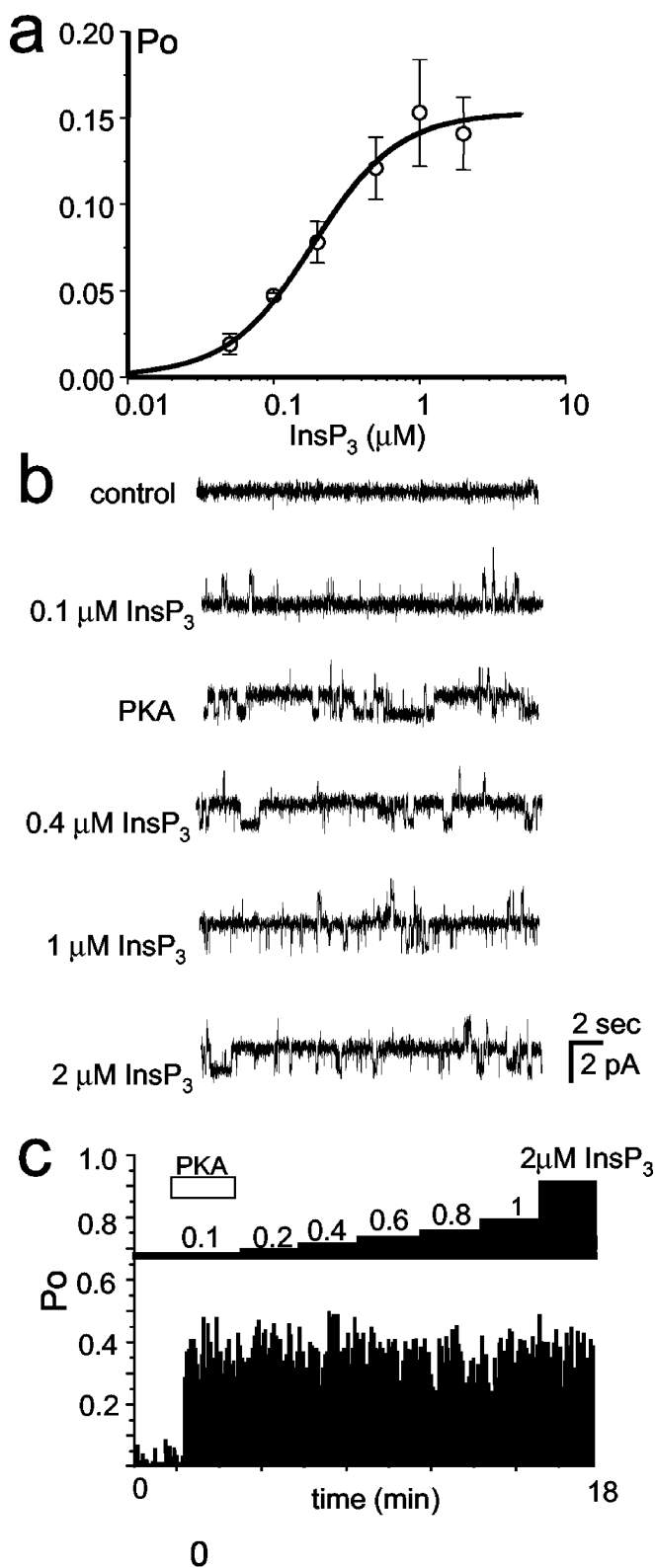


**Figure 10.** Apparent affinity of InsP<sub>3</sub>R for InsP<sub>3</sub> is increased by PKA phosphorylation. *a*, The InsP<sub>3</sub> dependence of InsP<sub>3</sub>R in control conditions. The InsP<sub>3</sub>R1 P<sub>0</sub> values measured in several independent experiments were averaged together at each InsP<sub>3</sub> concentration as described in Materials and Methods and shown as mean ± SE for high-activity InsP<sub>3</sub>R1 ( $n = 3$ ; open circles). The averaged data were fitted by the equation modified from Lupu et al. (1998), as explained in Materials and Methods. The parameters of optimal fit (smooth curve) yielded  $K_{\text{InsP}_3} = 0.19 \mu\text{M}$ ;  $n = 1.47$ ;  $P_{\text{max}} = 0.154$ . *b*, *c*, Effect of PKA on the InsP<sub>3</sub>R1 InsP<sub>3</sub> dependence. *b*, Each trace corresponds to 20 sec of recombinant InsP<sub>3</sub>R1 current recordings from the same experiment. The experiment was performed in the presence of pCa 6.7 and 0.5 mM MgATP in the *cis* (cyto-

poorly understood. The potency of InsP<sub>3</sub> to release Ca<sup>2+</sup> from cerebellar microsomes was reduced 10-fold because of PKA phosphorylation (Supattapone et al., 1988; Cameron et al., 1995), indicating that the link between InsP<sub>3</sub> binding and channel opening is impaired in PKA-phosphorylated InsP<sub>3</sub>R1. To the contrary, data from other groups, obtained with cerebellar microsomes (Volpe and Alderson-Lang, 1990), with the proteoliposomes containing purified cerebellar InsP<sub>3</sub>R1 (Nakade et al., 1994), or with permeabilized SH-SY5Y neuroblastoma cells (Wojcikiewicz and Luo, 1998), indicated that InsP<sub>3</sub>-mediated Ca<sup>2+</sup> release is facilitated by PKA phosphorylation. The reasons for these conflicting results are not clear and more importantly, interpretation of these data are obscured by changes in the rate of Ca<sup>2+</sup> uptake into the stores, known to be affected by PKA phosphorylation.

In this study, the effects of PKA on InsP<sub>3</sub>R1 function were evaluated using the planar lipid bilayer reconstitution technique. This technique has been used previously to analyze effects of PKA on skeletal and cardiac ryanodine receptors (RyanRs) (Hain et al., 1995; Marx et al., 2000). The planar lipid bilayer reconstitution method offers a number of advantages compared with previously used Ca<sup>2+</sup> flux measurements. In planar lipid bilayer experiments, we were able to describe the functional effects of InsP<sub>3</sub>R1 phosphorylation by PKA in well defined experimental conditions, such as, for example, different cytosolic Ca<sup>2+</sup> (Fig. 9) and InsP<sub>3</sub> (Fig. 10) concentrations. Most importantly, in planar lipid bilayer experiments, effects of PKA on InsP<sub>3</sub>R1 can be studied in isolation from effects on Ca<sup>2+</sup>-ATPase and other signaling proteins. From our experiments, we concluded that PKA activates and PP1 $\alpha$  inhibits the activity of InsP<sub>3</sub>R1 (Fig. 8). Interestingly, similar functional effects of PKA and PP1 on skeletal and cardiac RyanRs has been described previously (Hain et al., 1995; Marx et al., 2000), suggesting that both families of intracellular Ca<sup>2+</sup> release channels are subject to similar modulation by PKA/PP1. Activation of InsP<sub>3</sub>R1 by PKA resulted from an increase in InsP<sub>3</sub>R1 sensitivity to InsP<sub>3</sub> activation (Fig. 10), with minimal effect on InsP<sub>3</sub>R1 Ca<sup>2+</sup> dependence (Fig. 9). The recombinant InsP<sub>3</sub>R1 used in our studies corresponds to neuronal InsP<sub>3</sub>R1 isoform (Mignery et al., 1990). Future studies will be required to test the effects of PKA on non-neuronal InsP<sub>3</sub>R1 isoform. These experiments will be enabled by functional expression of both InsP<sub>3</sub>R1 isoforms in Sf9 cells (Tu et al., 2002). Additional experiments will also be needed to evaluate the role of two PKA phosphorylation sites in control of InsP<sub>3</sub>R1 activity. These studies will require generation of InsP<sub>3</sub>R1 point mutations in S1755 and S1589 PKA phosphorylation sites.

#### InsP<sub>3</sub>R1 as a core of macromolecular signaling complex

An emerging theme in signal transduction is the association of signaling molecules in macromolecular signaling complexes. Direct association of upstream and downstream signaling components increases the speed, efficiency, and specificity of signal transduction. Association between signaling molecules is mediated frequently by adaptor proteins. For example, recent data suggested that cardiac RyanR2 forms a complex with cAMP-dependent kinase-anchoring protein 6 (AKAP6)/PKA, spinophilin/PP1, and PR130/PP2A, and

←

solic) chamber at InsP<sub>3</sub> concentrations from 100 nM to 2 μM. Addition of PKA directly to the bilayer increased the InsP<sub>3</sub>R1 activity (third trace). The filter frequency is 200 Hz for all traces shown. *c*, The InsP<sub>3</sub>R1 P<sub>0</sub> was calculated for a 5 sec window of time and was plotted for the duration of an experiment. Changes in InsP<sub>3</sub> concentration (from 100 nM to 2 μM as indicated) in the *cis* chamber and the time of PKA addition to the bilayer are shown by the bar diagram. The data shown in *b* and *c* are from the same experiment.

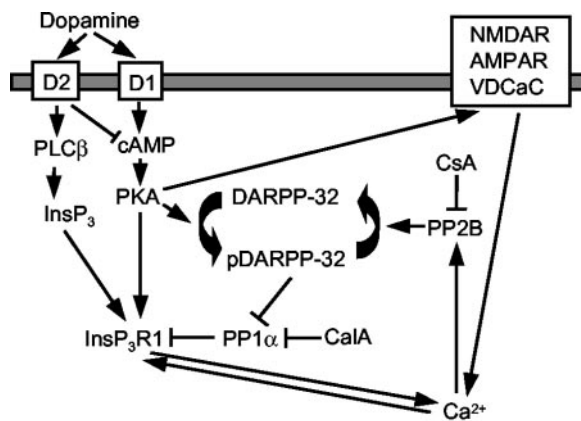


**Figure 11.** Model of InsP<sub>3</sub>R1 participation in cross talk between cAMP and Ca<sup>2+</sup> signaling pathways during dopaminergic signaling in the neostriatum. The model drawing is adapted from Greengard et al. (1999). Arrows depict activating influence, whereas blocking arrows (—) depict inhibitory influence. The points of cyclosporine A (CsA) and calyculin A (CalA) interference with the phosphorylated state of neostriatal InsP<sub>3</sub>R1 in our experiments are indicated. See Discussion. NMDAR, NMDA receptor; AMPAR, AMPA receptor; VDCaC, Voltage-gated Ca<sup>2+</sup> channels.

that cardiac RyanR2 is activated by PKA phosphorylation and inhibited by PP1 dephosphorylation (Marx et al., 2000, 2001). Association of AKAP6, spinophilin, and PR130 with RyanR2 is mediated via noncanonical leucine–isoleucine zipper (LIZ) motifs (Marx et al., 2001). Our sequence analysis (data not shown) reveals that putative AKAP-binding LIZ motif is also present in the InsP<sub>3</sub>R1 sequence, but that the spinophilin and PR130-binding LIZ motifs are absent. Future studies will be needed to clarify the role of putative AKAP-binding LIZ motif in the InsP<sub>3</sub>R1 sequence.

In this study, we discovered direct and specific association of the C-terminal portion of InsP<sub>3</sub>R1 with PP1 $\alpha$  (Figs. 1–3) and show that this association facilitates dephosphorylation of PKA-phosphorylated InsP<sub>3</sub>R1 (Fig. 5). The association of InsP<sub>3</sub>R1 with FKBP12/calcineurin has been reported previously (Cameron et al., 1995, 1997; but see Bultynck et al., 2001a,b). The N-terminal of InsP<sub>3</sub>R1 binds to the adaptor protein Homer (Tu et al., 1998) and to Ca<sup>2+</sup>-binding protein caldendrin, which affects InsP<sub>3</sub>R1 gating (Yang et al., 2002). The middle coupling domain of InsP<sub>3</sub>R1 binds to calmodulin (Yamada et al., 1995). Future experiments will likely lead to identification of additional InsP<sub>3</sub>R1-binding partners. Nevertheless, it is becoming apparent that InsP<sub>3</sub>R1 forms a core of macromolecular signaling complex that includes a number of associated signaling proteins, some of which are able to modulate the InsP<sub>3</sub>R1 activity.

### Potential role of InsP<sub>3</sub>R1 in cross talk between Ca<sup>2+</sup> and cAMP signaling in neostriatum

A cross talk between cAMP and Ca<sup>2+</sup>-signaling pathways plays an important role in dopaminergic signaling in the neostriatum (Greengard et al., 1999). From our results, we hypothesize that InsP<sub>3</sub>R1 may participate in this process (Fig. 11). We reason that because of direct association between InsP<sub>3</sub>R1 and PP1 $\alpha$  (Figs. 1–4), a fraction of PKA-phosphorylated InsP<sub>3</sub>R1 in the neostriatum is kept below 40% (Fig. 6b). The effect of calyculin A and cyclosporine A on the InsP<sub>3</sub>R1 phosphorylated state (Fig. 6) indicates that even under resting conditions, the phosphorylated state of neostriatal InsP<sub>3</sub>R1 is determined by a balance between competing activities of kinases and phosphatases. A similar conclusion has been reached previously regarding the levels of DARPP-32 phosphorylation (Nishi et al., 1997). The PKA-

phosphorylated state of neostriatal InsP<sub>3</sub>R1 appears to depend on PP1 and PP2B activity but not on PP2A activity, because 10 nM okadaic acid had only a minor effect on the InsP<sub>3</sub>R1 phosphorylated state in our experiments (Figs. 6, 7c). The effect of calyculin A on InsP<sub>3</sub>R1 phosphorylation is likely attributable to direct inhibition of PP1 phosphatase, but the effect of cyclosporine A is likely mediated by inhibition of PP2B phosphatase, which controls the phosphorylation state of DARPP-32 (Nishi et al., 1999) (Fig. 11).

We propose that after release of dopamine and stimulation of D1 receptors, an increase in the cAMP level leads to activation of PKA and transient phosphorylation of the InsP<sub>3</sub>R1 (Fig. 7a) and DARPP-32 (Nishi et al., 1997; Greengard et al., 1999) proteins. Phosphorylation of InsP<sub>3</sub>R1 by PKA promotes InsP<sub>3</sub>R1 activation (Fig. 8) and release of Ca<sup>2+</sup> from intracellular stores. An increase in intracellular Ca<sup>2+</sup> leads to activation of calcineurin (PP2B), which dephosphorylates DARPP-32 protein and closes the negative feedback loop (Nishi et al., 1997; Greengard et al., 1999). After dephosphorylation of DARPP-32, the InsP<sub>3</sub>R1-associated PP1 $\alpha$  is able to dephosphorylate neostriatal InsP<sub>3</sub>R1, returning it to the initial state (Fig. 7a). A similar negative feedback mechanism has been proposed previously to involve Ca<sup>2+</sup> influx via NMDA receptors (Blank et al., 1997; Cepeda et al., 1998; Snyder et al., 1998), AMPA receptors (Yan et al., 1999), and voltage-gated Ca<sup>2+</sup> channels (Surmeier et al., 1995; Cepeda et al., 1998). Influx of Ca<sup>2+</sup> via plasma membrane channels may have an additive effect with Ca<sup>2+</sup> released via InsP<sub>3</sub>R1 by directly activating calcineurin, or it may have a synergistic effect caused by the potentiating effect of Ca<sup>2+</sup> on the InsP<sub>3</sub>R1 (Bezprozvanny et al., 1991) (Fig. 11). The proposed model may also help to explain the antagonism between D2 and D1 dopamine receptors co-expressed in a subpopulation of neostriatal medium spiny neurons (Surmeier et al., 1996; Nishi et al., 1997; Lindskog et al., 1999). The activation of PLC $\beta$  via D2 receptors (Vallar et al., 1990; Hernandez-Lopez et al., 2000) causes an increase in InsP<sub>3</sub> levels that can boost the InsP<sub>3</sub>R1–Ca<sup>2+</sup>–PP2B negative feedback loop (Fig. 11). In this study, we focused on cross talk between dopamine/cAMP and Ca<sup>2+</sup> signaling systems in the neostriatum. A similar model may also be relevant in the context of synaptic plasticity in the hippocampus and in other regions of the brain, with the PP1-inhibitor 1 (Allen et al., 2000) playing the role analogous to the role of DARPP-32 in the neostriatum.

*Note added on proof.* While this paper was prepared for publication, association of InsP<sub>3</sub>R1 with PKA, PP1, and PP2A was reported by deSouza et al. (2002).

### References

- Allen PB, Hvalby O, Jensen V, Errington ML, Ramsay M, Chaudhry FA, Bliss TV, Storm-Mathisen J, Morris RG, Andersen P, Greengard P (2000) Protein phosphatase-1 regulation in the induction of long-term potentiation: heterogeneous molecular mechanisms. *J Neurosci* 20:3537–3543.
- Berridge MJ (1993) Inositol trisphosphate and calcium signalling. *Nature* 361:315–325.
- Berridge MJ (1998) Neuronal calcium signaling. *Neuron* 21:13–26.
- Bezprozvanny I, Ehrlich BE (1993) ATP modulates the function of inositol 1,4,5-trisphosphate-gated channels at two sites. *Neuron* 10:1175–1184.
- Bezprozvanny I, Ehrlich BE (1995) The inositol 1,4,5-trisphosphate (InsP<sub>3</sub>) receptor. *J Membr Biol* 145:205–216.
- Bezprozvanny I, Watras J, Ehrlich BE (1991) Bell-shaped calcium-response curves of Ins(1,4,5)P<sub>3</sub>- and calcium-gated channels from endoplasmic reticulum of cerebellum. *Nature* 351:751–754.
- Blank T, Nijholt I, Teichert U, Kugler H, Behrsing H, Fienberg A, Greengard P, Spiess J (1997) The phosphoprotein DARPP-32 mediates cAMP-dependent potentiation of striatal N-methyl-D-aspartate responses. *Proc Natl Acad Sci USA* 94:14859–14864.

- Blondel O, Takeda J, Janssen H, Seino S, Bell GI (1993) Sequence and functional characterization of a third inositol trisphosphate receptor subtype, IP<sub>3</sub>R-3, expressed in pancreatic islets, gastrointestinal tract, and other tissues. *J Biol Chem* 268:11356–11363.
- Bultynck G, Rossi D, Callewaert G, Missiaen L, Sorrentino V, Parys JB, De Smedt H (2001a) The conserved sites for the FK506-binding proteins in ryanodine receptors and inositol 1,4,5-trisphosphate receptors are structurally and functionally different. *J Biol Chem* 276:47715–47724.
- Bultynck G, De Smet P, Rossi D, Callewaert G, Missiaen L, Sorrentino V, De Smedt H, Parys JB (2001b) Characterization and mapping of the 12 kDa FK506-binding protein (FKBP12)-binding site on different isoforms of the ryanodine receptor and of the inositol 1,4,5-trisphosphate receptor. *Biochem J* 354:413–422.
- Cameron AM, Steiner JP, Roskams AJ, Ali SM, Ronnett GV, Snyder SH (1995) Calcineurin associated with the inositol 1,4,5-trisphosphate receptor-FKBP12 complex modulates Ca<sup>2+</sup> flux. *Cell* 83:463–472.
- Cameron AM, Nucifora Jr FC, Fung ET, Livingston DJ, Aldape RA, Ross CA, Snyder SH (1997) FKBP12 binds the inositol 1,4,5-trisphosphate receptor at leucine-proline (1400–1401) and anchors calcineurin to this FK506-like domain. *J Biol Chem* 272:27582–27588.
- Cepeda C, Colwell CS, Itri JN, Chandler SH, Levine MS (1998) Dopaminergic modulation of NMDA-induced whole cell currents in neostriatal neurons in slices: contribution of calcium conductances. *J Neurophysiol* 79:82–94.
- Colquhoun D, Hawkes AG (1983) The principles of stochastic interpretation of ion-channel mechanisms. In: *Single-channel recording* (Sakmann B, Neher E, eds), pp 135–174. New York: Plenum.
- da Cruz e Silva EF, Fox CA, Ouimet CC, Gustafson E, Watson SJ, Greengard P (1995) Differential expression of protein phosphatase 1 isoforms in mammalian brain. *J Neurosci* 15:3375–3389.
- Danoff SK, Ferris CD, Donath C, Fischer GA, Munemitsu S, Ullrich A, Snyder SH, Ross CA (1991) Inositol 1,4,5-trisphosphate receptors: distinct neuronal and nonneuronal forms derived by alternative splicing differ in phosphorylation. *Proc Natl Acad Sci USA* 88:2951–2955.
- DeSouza N, Reiken S, Ondrias K, Yang YM, Matkovich S, Marks AR (2002) Protein kinase A and two phosphatases are components of the inositol 1,4,5-trisphosphate receptor macromolecular signaling complex. *J Biol Chem* 277:39397–39400.
- Fabiato A (1988) Computer programs for calculating total from specified free or free from specified total ionic concentrations in aqueous solutions containing multiple metals and ligands. *Methods Enzymol* 157:378–417.
- Ferris CD, Haganir RL, Snyder SH (1990) Calcium flux mediated by purified inositol 1,4,5-trisphosphate receptor in reconstituted lipid vesicles is allosterically regulated by adenine nucleotides. *Proc Natl Acad Sci USA* 87:2147–2151.
- Ferris CD, Cameron AM, Brecht DS, Haganir RL, Snyder SH (1991a) Inositol 1,4,5-trisphosphate receptor is phosphorylated by cyclic AMP-dependent protein kinase at serines 1755 and 1589. *Biochem Biophys Res Commun* 175:192–198.
- Ferris CD, Haganir RL, Brecht DS, Cameron AM, Snyder SH (1991b) Inositol trisphosphate receptor-phosphorylation by protein kinase-C and calcium calmodulin-dependent protein kinases in reconstituted lipid vesicles. *Proc Natl Acad Sci USA* 88:2232–2235.
- Finch EA, Turner TJ, Goldin SM (1991) Calcium as a coagonist of inositol 1,4,5-trisphosphate-induced calcium release. *Science* 252:443–446.
- Furuichi T, Kohda K, Miyawaki A, Mikoshiba K (1994) Intracellular channels. *Curr Opin Neurobiol* 4:294–303.
- Greengard P, Allen PB, Nairn AC (1999) Beyond the dopamine receptor: the DARPP-32/protein phosphatase-1 cascade. *Neuron* 23:435–447.
- Hain J, Onoue H, Mayrleitner M, Fleischer S, Schindler H (1995) Phosphorylation modulates the function of the calcium release channel of sarcoplasmic reticulum from cardiac muscle. *J Biol Chem* 270:2074–2081.
- Hata Y, Butz S, Sudhof TC (1996) CASK: a novel dlg/PSD95 homolog with an N-terminal calmodulin-dependent protein kinase domain identified by interaction with neuexins. *J Neurosci* 16:2488–2494.
- Haug LS, Jensen V, Hvalby O, Walaas SI, Ostvold AC (1999) Phosphorylation of the inositol 1,4,5-trisphosphate receptor by cyclic nucleotide-dependent kinases in vitro and in rat cerebellar slices in situ. *J Biol Chem* 274:7467–7473.
- Hernandez-Lopez S, Tkatch T, Perez-Garci E, Galarraga E, Bargas J, Hamm H, Surmeier DJ (2000) D2 dopamine receptors in striatal medium spiny neurons reduce L-type Ca<sup>2+</sup> currents and excitability via a novel PLC[ $\beta$ ]1-IP3-calcineurin-signaling cascade. *J Neurosci* 20:8987–8995.
- Horn R (1991) Estimating the number of channels in patch recordings. *Biophys J* 60:433–439.
- Iino M (1990) Biphasic Ca<sup>2+</sup> dependence of inositol 1,4,5-trisphosphate-induced Ca release in smooth muscle cells of the guinea pig *taenia caeci*. *J Gen Physiol* 95:1103–1122.
- Iino M (1991) Effects of adenine nucleotides on inositol 1,4,5-trisphosphate-induced calcium release in vascular smooth muscle cells. *J Gen Physiol* 98:681–698.
- Jones DH, Matus AI (1974) Isolation of synaptic plasma membrane from brain by combined flotation-sedimentation density gradient centrifugation. *Biochim Biophys Acta* 356:276–287.
- Kaznacheeva E, Lupu VD, Bezprozvanny I (1998) Single-channel properties of inositol (1,4,5)-trisphosphate receptor heterologously expressed in HEK-293 cells. *J Gen Physiol* 111:847–856.
- Lindskog M, Svenningsson P, Fredholm BB, Greengard P, Fisone G (1999) Activation of dopamine D2 receptors decreases DARPP-32 phosphorylation in striatonigral and striatopallidal projection neurons via different mechanisms. *Neuroscience* 88:1005–1008.
- Lupu VD, Kaznacheeva E, Krishna UM, Falck JR, Bezprozvanny I (1998) Functional coupling of phosphatidylinositol 4,5-bisphosphate to inositol 1,4,5-trisphosphate receptor. *J Biol Chem* 273:14067–14070.
- Maeda N, Niinobe M, Mikoshiba K (1990) A cerebellar Purkinje cell marker P<sub>400</sub> protein is an inositol 1,4,5-trisphosphate (InsP<sub>3</sub>) receptor protein. Purification and characterization of InsP<sub>3</sub> receptor complex. *EMBO J* 9:61–67.
- Marx SO, Reiken S, Hisamatsu Y, Jayaraman T, Burkhoff D, Rosembly N, Marks AR (2000) PKA phosphorylation dissociates FKBP12.6 from the calcium release channel (ryanodine receptor): defective regulation in failing hearts. *Cell* 101:365–376.
- Marx SO, Reiken S, Hisamatsu Y, Gaburjakova M, Gaburjakova J, Yang YM, Rosembly N, Marks AR (2001) Phosphorylation-dependent regulation of ryanodine receptors: a novel role for leucine/isoleucine zippers. *J Cell Biol* 153:699–708.
- Matsumoto M, Nakagawa T, Inoue T, Nagata E, Tanaka K, Takano H, Minowa O, Kuno J, Sakakibara S, Yamada M, Yoneshima H, Miyawaki A, Fukuuchi Y, Furuichi T, Okano H, Mikoshiba K, Noda T (1996) Ataxia and epileptic seizures in mice lacking type 1 inositol 1,4,5-trisphosphate receptor. *Nature* 379:168–171.
- Maximov A, Sudhof TC, Bezprozvanny I (1999) Association of neuronal calcium channels with modular adaptor proteins. *J Biol Chem* 274:24453–24456.
- Mignery GA, Newton CL, Archer BT, Sudhof TC (1990) Structure and expression of the rat inositol 1,4,5-trisphosphate receptor. *J Biol Chem* 265:12679–12685.
- Nakade S, Rhee SK, Hamanaka H, Mikoshiba K (1994) Cyclic AMP-dependent phosphorylation of an immunopurified homotetrameric inositol 1,4,5-trisphosphate receptor (type I) increases Ca<sup>2+</sup> flux in reconstituted vesicles. *J Biol Chem* 269:6735–6742.
- Nishi A, Snyder GL, Greengard P (1997) Bidirectional regulation of DARPP-32 phosphorylation by dopamine. *J Neurosci* 17:8147–8155.
- Nishi A, Snyder GL, Nairn AC, Greengard P (1999) Role of calcineurin and protein phosphatase-2A in the regulation of DARPP-32 dephosphorylation in neostriatal neurons. *J Neurochem* 72:2015–2021.
- Nosyreva E, Miyakawa T, Wang Z, Glouchankova L, Mizushima A, Iino M, Bezprozvanny I (2002) The high affinity calcium-calmodulin-binding site does not play a role in modulation of type 1 inositol (1,4,5)-trisphosphate receptor function by calcium and calmodulin. *Biochem J* 365:659–667.
- Ouimet CC, da Cruz e Silva EF, Greengard P (1995) The  $\alpha$  and  $\gamma$ 1 isoforms of protein phosphatase 1 are highly and specifically concentrated in dendritic spines. *Proc Natl Acad Sci USA* 92:3396–3400.
- Pieper AA, Brat DJ, O'Hearn E, Krug DK, Kaplin AI, Takahashi K, Greenberg JH, Ginty D, Molliver ME, Snyder SH (2001) Differential neuronal localizations and dynamics of phosphorylated and unphosphorylated type 1 inositol 1,4,5-trisphosphate receptors. *Neuroscience* 102:433–444.
- Sharp AH, Dawson TM, Ross CA, Fotuhi M, Mourey RJ, Snyder SH (1993a) Inositol 1,4,5-trisphosphate receptors: immunohistochemical localization to discrete areas of rat central nervous system. *Neuroscience* 53:927–942.
- Sharp AH, McPherson PS, Dawson TM, Aoki C, Campbell KP, Snyder SH

- (1993b) Differential immunohistochemical localization of inositol 1,4,5-trisphosphate- and ryanodine-sensitive Ca<sup>2+</sup> release channels in rat brain. *J Neurosci* 13:3051–3063.
- Sipma H, De Smet P, Sienaert I, Vanlingen S, Missiaen L, Parys JB, De Smedt H (1999) Modulation of inositol 1,4,5-trisphosphate binding to the recombinant ligand-binding site of the type-1 inositol 1,4,5-trisphosphate receptor by Ca<sup>2+</sup> and calmodulin. *J Biol Chem* 274:12157–12162.
- Snyder GL, Fienberg AA, Huganir RL, Greengard P (1998) A dopamine/D1 receptor/protein kinase A/dopamine- and cAMP-regulated phosphoprotein (M<sub>r</sub> 32 kDa)/protein phosphatase-1 pathway regulates dephosphorylation of the NMDA receptor. *J Neurosci* 18:10297–10303.
- Sudhof TC, Newton CL, Archer BT, Ushkaryov YA, Mignery GA (1991) Structure of a novel InsP<sub>3</sub> receptor. *EMBO J* 10:3199–3206.
- Supattapone S, Danoff SK, Theibert A, Joseph SK, Steiner J, Snyder SH (1988) Cyclic AMP-dependent phosphorylation of a brain inositol trisphosphate receptor decreases its release of calcium. *Proc Natl Acad Sci USA* 85:8747–8750.
- Surmeier DJ, Vargas J, Hemmings Jr HC, Nairn AC, Greengard P (1995) Modulation of calcium currents by a D1 dopaminergic protein kinase/phosphatase cascade in rat neostriatal neurons. *Neuron* 14:385–397.
- Surmeier DJ, Song WJ, Yan Z (1996) Coordinated expression of dopamine receptors in neostriatal medium spiny neurons. *J Neurosci* 16:6579–6591.
- Taylor CW, Genazzani AA, Morris SA (1999) Expression of inositol trisphosphate receptors. *Cell Calcium* 26:237–251.
- Thrower EC, Hagar RE, Ehrlich BE (2001) Regulation of Ins(1,4,5)P<sub>3</sub> receptor isoforms by endogenous modulators. *Trends Pharmacol Sci* 22:580–586.
- Tu H, Miyakawa T, Wang Z, Glouchankova L, Iino M, Bezprozvanny I (2002) Functional characterization of the type I inositol 1,4,5-trisphosphate receptor coupling domain SII(+/-) splice variants and the *opisthotonos* mutant form. *Biophys J* 82:1995–2004.
- Tu JC, Xiao B, Yuan JP, Lanahan AA, Leoffert K, Li M, Linden DJ, Worley PF (1998) Homer binds a novel proline-rich motif and links group 1 metabotropic glutamate receptors with IP<sub>3</sub> receptors. *Neuron* 21:717–726.
- Vallar L, Muca C, Magni M, Albert P, Buzow J, Meldolesi J, Civelli O (1990) Differential coupling of dopaminergic D2 receptors expressed in different cell types. Stimulation of phosphatidylinositol 4,5-bisphosphate hydrolysis in LtK-fibroblasts, hyperpolarization, and cytosolic-free Ca<sup>2+</sup> concentration decrease in GH4C1 cells. *J Biol Chem* 265:10320–10326.
- Volpe P, Alderson-Lang BH (1990) Regulation of inositol 1,4,5-trisphosphate-induced Ca<sup>2+</sup> release. II. Effect of cAMP-dependent protein kinase. *Am J Physiol* 258:C1086–C1091.
- Walaas SI, Nairn AC, Greengard P (1986) PCPP-260, a Purkinje cell-specific cyclic AMP-regulated membrane phosphoprotein of M<sub>r</sub> 260,000. *J Neurosci* 6:954–961.
- Wojcikiewicz RJ, Luo SG (1998) Phosphorylation of inositol 1,4,5-trisphosphate receptors by cAMP-dependent protein kinase. Type I, II, and III receptors are differentially susceptible to phosphorylation and are phosphorylated in intact cells. *J Biol Chem* 273:5670–5677.
- Yamada M, Miyawaki A, Saito K, Nakajima T, Yamamoto-Hino M, Ryo Y, Furuichi T, Mikoshiba K (1995) The calmodulin-binding domain in the mouse type I inositol 1,4,5-trisphosphate receptor. *Biochem J* 308:83–88.
- Yan Z, Hsieh-Wilson L, Feng J, Tomizawa K, Allen PB, Fienberg AA, Nairn AC, Greengard P (1999) Protein phosphatase 1 modulation of neostriatal AMPA channels: regulation by DARPP-32 and spinophilin. *Nat Neurosci* 2:13–17.
- Yang J, McBride S, Mak DO, Vardi N, Palczewski K, Haeseleer F, Foscett JK (2002) Identification of a family of calcium sensors as protein ligands of inositol trisphosphate receptor Ca<sup>2+</sup> release channels. *Proc Natl Acad Sci USA* 7:7–12.